

The Relation Between AGN and Host Galaxy Properties: I. Obscured AGN reside in disturbed hosts at $0 < z < 4$

NINA BONAVENTURA,¹ JIANWEI LYU (吕建伟),¹ GEORGE H. RIEKE,¹ STACEY ALBERTS,¹ CHRISTOPHER N. A. WILLMER,¹
PABLO G. PÉREZ-GONZÁLEZ,² ANDREW J. BUNKER,³ MEREDITH STONE,¹ FRANCESCO D'EUGENIO,^{4,5}
CHRISTINA C. WILLIAMS,^{6,1} MICHAEL V. MASEDA,⁷ CHRIS J. WILLOTT,⁸ ZHIYUAN JI,⁹ WILLIAM M. BAKER,^{10,11}
STEFANO CARNIANI,¹² STEPHANE CHARLOT,¹³ JACOPO CHEVALLARD,³ EMMA CURTIS-LAKE,¹⁴ DANIEL J. EISENSTEIN,¹⁵
KEVIN HAINLINE,⁹ RYAN HAUSEN,¹⁶ ERICA J. NELSON,¹⁷ MARCIA J. RIEKE,⁹ BRANT ROBERTSON,¹⁸ AND IRENE SHIVAEI²

¹Steward Observatory, University of Arizona, 933 North Cherry Avenue, Tucson, AZ 85721, USA

²Centro de Astrobiología (CAB), CSIC-INTA, Ctra. de Ajalvir km 4, Torrejón de Ardoz, E-28850, Madrid, Spain

³Department of Physics, University of Oxford, Denys Wilkinson Building, Keble Road, Oxford OX1 3RH, UK

⁴Kavli Institute for Cosmology, University of Cambridge, Madingley Road, Cambridge, CB3 0HA, UK

⁵Cavendish Laboratory, University of Cambridge, 19 JJ Thomson Avenue, Cambridge, CB3 0HE, UK

⁶NSF's National Optical-Infrared Astronomy Research Laboratory, 950 North Cherry Avenue, Tucson, AZ 85719, USA

⁷Department of Astronomy, University of Wisconsin-Madison, 475 N. Charter St., Madison, WI 53706 USA

⁸NRC Herzberg, 5071 West Saanich Rd, Victoria, BC V9E 2E7, Canada

⁹Steward Observatory, University of Arizona, 933 N. Cherry Ave, Tucson, AZ 85721, USA

¹⁰Kavli Institute for Cosmology, University of Cambridge, Madingley Road, Cambridge CB3 0HA, UK

¹¹Cavendish Laboratory, University of Cambridge, 19 JJ Thomson Avenue, Cambridge CB3 0HE, UK

¹²Scuola Normale Superiore, Piazza dei Cavalieri 7, I-56126 Pisa, Italy

¹³Sorbonne Université, UPMC-CNRS, UMR7095, Institut d'Astrophysique de Paris, F-75014 Paris, France

¹⁴Centre for Astrophysics Research, Department of Physics, Astronomy and Mathematics, University of Hertfordshire, Hatfield AL10 9AB, UK

¹⁵Center for Astrophysics — Harvard and Smithsonian, 60 Garden Street, Cambridge, MA 02138, USA

¹⁶Department of Physics and Astronomy, The Johns Hopkins University, 3400 N. Charles St., Baltimore, MD 21218, USA

¹⁷Department for Astrophysical and Planetary Science, University of Colorado, Boulder, CO 80309, USA

¹⁸Department of Astronomy and Astrophysics, University of California, Santa Cruz, 1156 High Street, Santa Cruz, CA 95064, USA

ABSTRACT

The morphology of a galaxy is a manifestation of the complex interplay of physical processes occurring within and around it, and therefore offers indirect clues to its formation and evolution. We use both visual classification and computer vision to verify the suspected connection between galaxy merging activity — as evidenced by a close/merging galaxy pair, or tidal features surrounding an apparently singular system — and AGN activity. This study makes use of JADES JWST/NIRCam imagery, along with an unprecedentedly complete sample of AGN built using JWST/MIRI photometry in the same field. This 0.9-25 μm dataset enables constraints on the host galaxy morphologies of the broadest possible range of AGN beyond $z \sim 1$, including heavily obscured examples missing from previous studies. We consider two AGN samples, one consisting of lightly to highly obscured X-ray-selected AGN (Lyu et al. 2022), and the other, presumed Compton-thick mid-infrared-bright/X-ray-faint AGN recently revealed by MIRI (Lyu et al. 2023). Both samples contain a significant fraction of host galaxies with disturbed morphologies at all redshifts sampled, and increasingly so towards higher redshift and AGN bolometric luminosity. The most obscured systems show the highest fraction of strongly disturbed host galaxies at $95 \pm 4\%$, followed by the moderately and unobscured/lightly obscured subsets at $78 \pm 6\%$ and $63 \pm 6.5\%$, respectively. From this pattern of disturbances, we conclude that mergers are common amongst obscured AGN, and that the obscured AGN phase may mark a period of significant SMBH growth. This finding presents tension with the leading model on AGN fueling mechanisms (Hopkins et al. 2014) that needs reconciling.

1. INTRODUCTION

In the hierarchical framework for large-scale structure formation in the Universe, a ‘cosmic cycle’ for galaxy formation and evolution is expected as a direct result of regularly occurring galaxy mergers (Hopkins & Hernquist 2006). In this picture, two gas-rich disk galaxies of similar masses merge to violently drive a nuclear inflow of gas towards the center of the system that triggers both starbursts and quasars ($L_{bol} \geq 10^{45}$ ergs/s), and therefore the simultaneous growth of black holes and stellar bulges in the centers of galaxies. Observational studies support this modeled co-evolution of galaxies with their central supermassive black holes (SMBHs), most famously the empirical $M - \sigma_{disp}$ relation showing the tight correlation between black hole mass and host galaxy velocity dispersion, demonstrating an undeniable link between the origin of galaxies and SMBHs (Ferrarese & Merritt 2000; Gebhardt et al. 2000; Tremaine et al. 2002). There is also the persistent coincidence of intensive star formation and embedded active nuclei in ultra-luminous infrared galaxies (ULIRGs) commonly associated with mergers (Sanders & Mirabel 1996; Jogee 2006).

It is predicted that for most of the lifetime of a merger, quasar activity is obscured at optical and (soft) X-ray wavelengths by a screen of gas and dust, manifesting in the appearance of an obscured, Type II quasar. The obscuring material could be confined to the nuclear region of the galaxy, and/or re-distributed to galaxy-wide scales by the triggering merger event (Hickox & Alexander 2018). This early obscured phase would then transition into the relatively brief, luminous, unobscured Type I quasar state once the radiative power of the black hole increases to the point of ejecting the obscuring material out and away, halting the ability of the active nucleus to sustain itself. At this point, a merger remnant would emerge in the form of a normal, passively evolving galaxy with a central stellar bulge and SMBH, with or without a surviving (or reformed) disk structure (Hopkins et al. 2009). As this process propagates across the galaxy population throughout cosmic time (and sometimes multiple times within the lifetime of a given galaxy/merger remnant), there is the expectation of a shift towards merger remnants with lower masses towards lower redshifts given the diminishing gas supply in the Universe; and, ultimately, to gas-poor elliptical galaxies (Hopkins & Hernquist 2006; Hickox & Alexander 2018; Hopkins et al. 2008; Blecha et al. 2018)).

The implication of this theoretical evolutionary scenario is that major galaxy mergers are largely responsible for the bulk of SMBH growth in the Universe (Hickox & Alexander 2018; Hopkins et al. 2008; Gilli et al. 2007); the alternative is that they are predominantly

fueled by stochastic processes, slowly over time, instead of through a series of short and dramatic episodes (Kormendy & Kennicutt 2004; Hopkins & Hernquist 2006; Hopkins et al. 2014). However, the observational evidence for the former conclusion is ambiguous (Treister et al. 2012; Zhiyuan et al. 2022) and the issue remains unresolved (see, e.g., Shah et al. 2020; Pierce et al. 2023; Hernández-Toledo et al. 2023; Villforth 2023). A further observational complexity is that Type I quasar host galaxies tend to lie on the star-forming fundamental plane (e.g., Xu et al. 2015; Zhang et al. 2016), rather than emerging from ULIRGs or lying in post-starburst, passively evolving galaxies, as might be expected from theoretical predictions. Finally, it is not clear if this generally accepted model for quasar evolution extends into the realm of Seyfert galaxies, defined by significantly lower luminosities and black hole masses than quasars (Hopkins et al. 2014).

Clues to this evolutionary scenario should lie in the host galaxy morphologies. There have been many programs to image the host galaxies of nearby and moderate redshift AGN and quasars; results are available for well over 200 systems (Kim et al. 2017). Although there are disagreements in the assignment of disturbances in individual cases, in general there is broad consistency among the studies that roughly 50% of the hosts appear disturbed, as illustrated in the comprehensive source-by-source summary by Kim et al. (2017). This agreement holds when different techniques are used, providing credibility to the assignments.

The great majority of the available studies have focused largely on Type I unobscured or lightly obscured AGN. However, the discovery of substantial numbers of Type II AGN in the SDSS (Zakamska et al. 2004) has enabled similar observations of their host galaxies. For example, Urbano-Mayorgas et al. (2019) report that, in a sample of 41 Type II quasars, $34^{+6}_9\%$ of the host galaxies are highly disturbed; they summarize the existing work as showing that 44 – 62% of Type II hosts are disturbed. Zakamska et al. (2019) present HST images of 10 extremely red quasars (ERQs)¹ and 6 Type II AGN, finding, respectively, that $(2 \pm 1)/10$ and $2/6$ of the hosts are disturbed. That is, it appears that these obscured AGN also show a significant fraction of disturbed hosts, as classified by the available methods. However, even the Type II samples discussed above do not include

¹ Zakamska et al. (2019) suggest that the relatively low number of disturbed hosts detected amongst the ERQs of their study may be due to the undetectability of faint merger signatures in the HST imagery utilized, e.g. if these systems are late-stage merger remnants and/or lie in very dusty host galaxies.

the most heavily obscured, Compton-thick ($N_H \geq 10^{24} \text{ cm}^{-2}$) AGN. A comprehensive study of the relation of host morphology to AGN obscuration needs to draw on the full range of AGN identification methods (Lyu et al. 2022), including those centered in the infrared that can detect AGN that are so obscured that their traces are hidden in other wavelength ranges. Earlier studies with HST and the *Spitzer* Infrared Camera (IRAC) attempted to compare the morphological properties of AGN selected by different methods (Zhiyuan et al. 2022), although those studies were only able to focus on AGN much brighter than those found by Lyu et al. (2023).

The possibility with the JWST Near-Infrared Camera (NIRCam) to study AGN host galaxy morphology at cosmic noon with unprecedented resolution and sensitivity at rest-optical wavelengths, provides the motivation for a new approach to these issues. Furthermore, the thoroughness of the AGN identification in the GOODS-South (GOODS-S) field, including the identification of a large sample of previously unknown obscured AGN out to high redshift (Lyu et al. 2022, 2023) allows for the study of the connection between large-scale morphological disturbances in an active galaxy and evidence of obscuration by dust and/or gas of its accretion disk. This paper initiates such a study. Here (Paper I), we present the details of our analysis of the JWST observations. In Paper II, we will supplement Paper I with additional multiwavelength data to support an evolutionary scenario for massive Seyfert galaxies implied by the results of the initial study.

Our discussion will develop as follows. Section 2 provides an overview of the new data we have used, specifically JWST/NIRCam images (Rieke et al. 2023) of both a pre-JWST X-ray-selected AGN sample (Lyu et al. 2022), and a JWST Mid-Infrared Instrument (MIRI) mid-IR-selected AGN sample. We also summarize the AGN identification methods relevant to our study. Section 3 describes the experimental design of our analysis, consisting of two distinct trials. Trial 1 takes a traditional approach to the analysis of the X-ray-selected subset of the AGN sample, utilizing the hydrogen absorbing column density, N_H , as the measure of AGN obscuration. We evaluate the host galaxy morphology for unobscured/light ($N_H < 10^{22} \text{ cm}^{-2}$), moderate ($10^{22} < N_H < 10^{23} \text{ cm}^{-2}$), and heavy X-ray obscuration ($N_H > 10^{23} \text{ cm}^{-2}$), and place the results in the context of existing studies. Given that the use of X-rays as a selection criterion biases the sample against the more heavily obscured objects (Del Moro et al. 2016; Lyu et al. 2022), Trial 2 analyzes the behavior of the host galaxies from the mid-IR-selected sample that should include

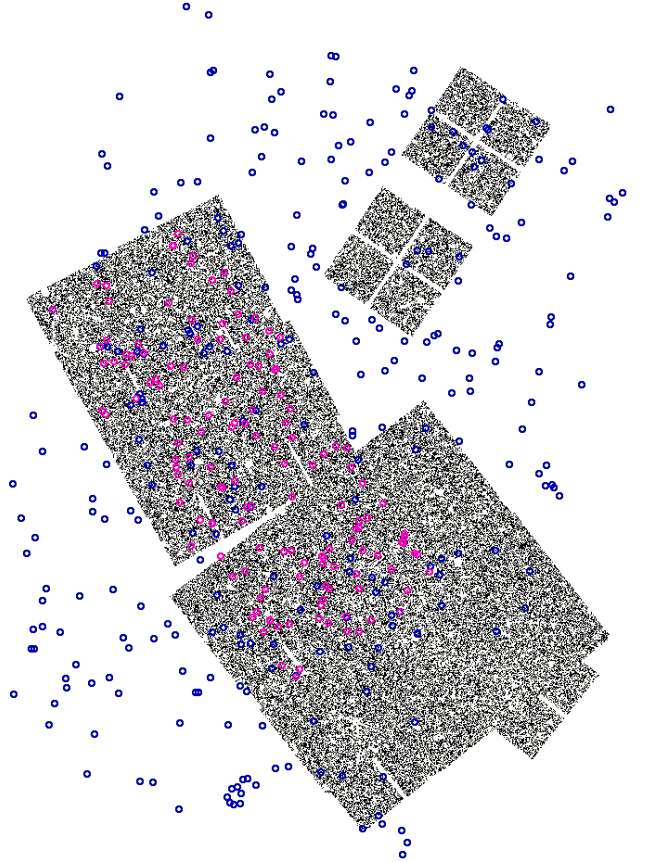


Figure 1. JADES V1 NIRCam F150W mosaic image containing the AGN sample targeted in GOODS-S/HUDF. Blue points mark the X-ray-selected AGN sample from Lyu et al. (2022), and the magenta points the mid-IR-selected MIRI AGN from Lyu et al. (2023)

a better and less-biased representation of the behavior of the most-obscured (presumed Compton-thick) AGN. Finally, we present the results of our analysis trials in Section 4, and a discussion of those results in Section 5.

The galaxy parameter values quoted in this paper are drawn directly from the SED analyses of Lyu et al. (2022) and Lyu et al. (2023), which adopt a slightly different cosmology: Lyu et al. (2022) assumes $\Omega_m = 0.27$ and $H_0 = 71 \text{ km s}^{-1} \text{ Mpc}^{-1}$, while (Lyu et al. 2023) assumes $\Omega_m = 0.287$ and $H_0 = 69.3 \text{ km s}^{-1} \text{ Mpc}^{-1}$.

2. SAMPLE AND DATA

This study is enabled by previous work to identify AGN in the GOODS-S region using ultra-deep *Chandra* and *Spitzer* imaging, now complemented by both the mid-IR identification of obscured AGN in the same region with JWST/MIRI, plus the ability to examine the host galaxies uniformly using JWST/NIRCam.

2.1. AGN sample

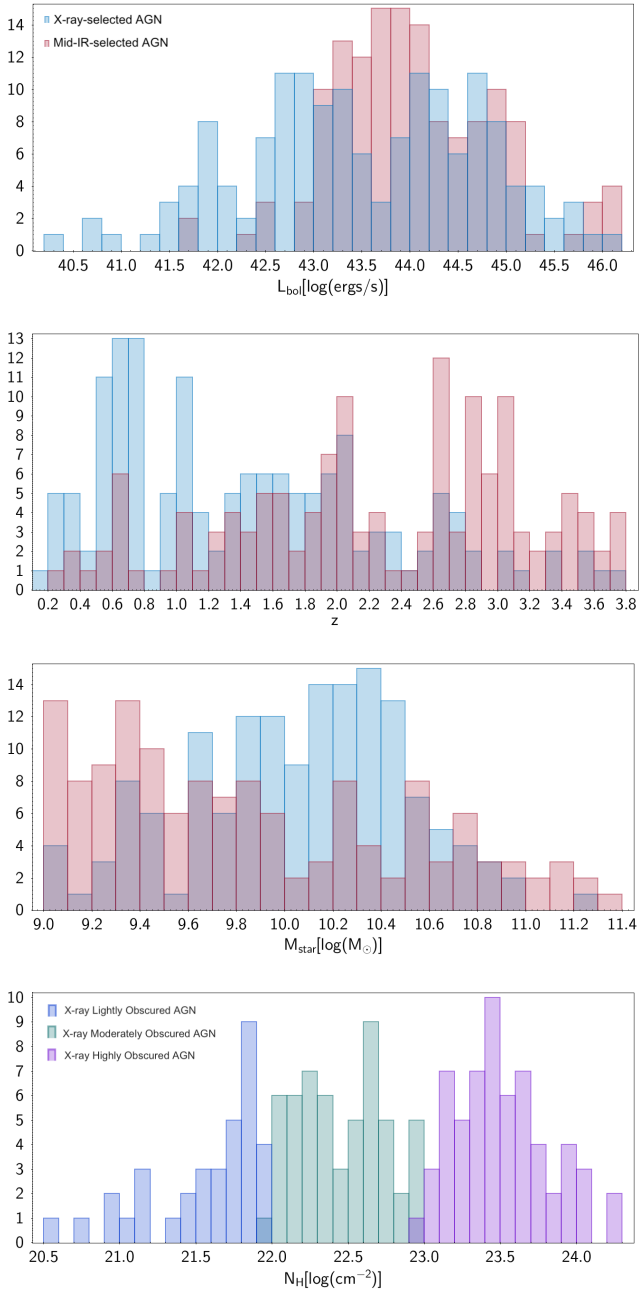


Figure 2. Histograms showing the distribution of the bolometric luminosities (L_{bol}), redshifts (z), and stellar masses (M_*) of the X-ray and MIRI AGN samples (Lyu et al. 2022, 2023); and the hydrogen absorbing column densities (N_H) used to measure obscuration in the X-ray AGN sample (Lyu et al. 2022). The L_{bol} values for the X-ray AGN sample represent the K-corrected intrinsic X-ray luminosity ($L_{x,int}$) (Lyu et al. 2022; Duras et al. 2020); and those for the MIRI AGN sample are based on the intrinsic, unobscured 4400 Å luminosity derived from the SED fitting procedure described in Lyu et al. (2023).

We gather sources from two data sets: the comprehensive census of GOODS-S/HUDF AGN detected at X-ray, optical, infrared, and/or radio wavelengths analyzed in Lyu et al. (2022) over an area of $\sim 170 \text{ arcmin}^2$; and a new sample of JWST/MIRI-detected AGN revealed by the SMILES MIRI GTO program (PI: G. Rieke) covering $\sim 34 \text{ arcmin}^2$ Lyu et al. (2023). Both Type I and II AGN are included in these samples, detected out to $z \sim 6$ via spectroscopic and/or photometric measurements, and are presented with a full set of SED-derived physical parameters.

2.1.1. X-ray AGN

The X-ray AGN sample was defined as all sources in the catalog of Lyu et al. (2022) for which the ratio of the 0.5–7 keV X-ray luminosity to the 3 GHz radio luminosity exceeds the physical threshold for stellar processes in a galaxy, and is therefore confidently attributed to AGN emission (Alberts et al. 2020). In fact, Lyu et al. (2022) discovered that the selection of AGN using the X-ray-to-radio luminosity ratio was the most effective of the multiwavelength selection methods they considered, until the recent multi-band JWST/MIRI measurements became available. We also restrict our sample to those X-ray-bright AGN with an available SED-derived N_H measurement from Luo et al. (2017). The vast majority of the resulting sample (hereafter the ‘pre-JWST’ AGN sample of Lyu et al. 2022) are optically faint, which conveniently minimizes AGN contamination in the rest-optical NIRCcam imagery we utilize for morphology analysis. The majority likewise lack a mid-IR counterpart in the SED analysis of Lyu et al. (2022), which appears to confirm the mostly faint intrinsic X-ray luminosities inferred from their SEDs, as photometric detection in the mid-IR requires a stronger intrinsic AGN luminosity than in the X-ray selection due to a higher competition from the host galaxy light in this wavelength regime of the SED (Hickox & Alexander 2018).

The properties of the X-ray AGN sample are shown in Figure 2. Of the total of 169 X-ray AGN meeting the criteria above, 151 were covered by the JADES/NIRCcam mosaic utilized in our analysis.

2.1.2. Mid-Infrared AGN

The mid-IR AGN sample constitutes the X-ray-faint subset of a batch of newly identified, JWST/MIRI-selected AGN from SMILES, a JWST Cycle 1 GTO program that has targeted the central region of GOODS-S with eight MIRI filters from 5.6 to 26 μm (Lyu et al. 2023). These sources were classified as AGN through an SED analysis consisting of JWST MIRI and NIRCcam photometry, in addition to HST photometry (Lyu et al. 2023). As we require the selected subset of sources to

lack a confident identification as X-ray AGN using the selection methods discussed in Lyu et al. (2022, 2023), these mid-IR sources are expected to represent the most heavily dust- and gas-obscured AGN in the sample.

The properties of the mid-IR AGN sample are shown in Figure 2 alongside those of the X-ray sample. Of the total of 182 mid-IR AGN meeting the criteria above, 138 were covered by the JADES/NIRCam mosaic utilized in our analysis.

2.2. JWST NIRCam Data

The NIRCam imaging utilized in this study was obtained as part of the JADES survey in JWST program 1180 (PI: Eisenstein), described in full detail in the JADES Data Release v1 paper (Rieke et al. 2023), as well as the JWST Extragalactic Medium-band Survey (JEMS) (JWST PID 1963) (Williams et al. 2023). JADES v1 NIRCam mosaic images of the GOODS-S/HUDF field are available in the 0.9 – 4.4 μm range in each of the following wide and medium filters: F090W, F115W, F150W, F200W, F277W, F335M, F356W, F410M, and F444W. Each mosaic image achieves 0.03"/pixel resolution and an AB magnitude depth of 29-30 (Rieke et al. 2023). We chose to work exclusively with the F150W NIRCam mosaic image for this study, as it proved to be the deepest and most resolved of the mosaics that also maximizes coverage of the sky positions of the AGN in our sample (see the Appendix for further details). It is displayed in Figure 1, showing the overlapping coverage of the AGN sample.

The NIRCam F150W filter has significant overlap with the HST WFC3 F160W band that has been widely utilized in various types of galaxy studies, from probing the peak of galaxy stellar emission at $z \sim 0$ to assisting in the capture of ‘Lyman break’ galaxies in the SEDs of $z > 9$ ‘J-band dropout’ galaxies (see, e.g., Henry et al. 2008). The observed effective wavelength of 1.5 μm of this filter translates to the rest-optical to rest-near-IR wavelength range of 0.33-1.5 μm for our $0 < z < 4$ AGN sample, which primarily probes stellar emission in the AGN host galaxies, at $\sim 5\times$ greater sensitivity than the HST F160W imaging band. While dust attenuation of starlight has been shown to bias measures of galaxy sizes and morphologies (see, e.g., Suess et al. 2022), we do not expect this effect to significantly impact the results and conclusions of the present study. The reason for this lies in our consideration of the non-parametric *shape* asymmetry of the AGN host galaxies as measured in the binary detection mask (also known as a ‘segmentation map’) associated with each galaxy image, composed of equally-weighted pixels (see Section 3.1.2 for details).

This contrasts with the more commonly used, classic asymmetry parameter that also measures variations in the brightness distribution of the pixel values directly drawn from the galaxy image (as well as parametric fits to galaxy surface brightness profiles to determine galaxy sizes, morphologies, and sub-structures). More specifically, given that the shape asymmetry parameter effectively traces the outline of a galaxy’s shape in a binary image, without regard to differences in pixel intensity, it would only be influenced by the effects of dust attenuation if the outer edges of an AGN host galaxy were significantly dusty, and the starlight significantly absorbed, fully or partially hiding the full extent and shape of the host galaxy.

The choice to analyze the AGN host galaxies using only image cutouts from the observed F150W JADES mosaic – which probes a range of rest-frame wavelengths as opposed to a single consistent rest-frame wavelength – was motivated by the following additional factors: 1) the limited overlap of our AGN sample with the mosaics exposed at the other NIRCam wavelengths sampled by JADES; 2) the obvious resolution degradation of the galaxy images at wavelengths longward of F150W due to the increasing PSF size²; and 3) the desire to avoid the extra sources of uncertainty that would be introduced to our analysis by comparing galaxy images extracted from mosaics in different filters.

3. METHODOLOGY

Methods to constrain galaxy morphologies historically range from the manual, visual classification of galaxy shapes that led most famously to Edwin Hubble’s ‘tuning fork’ sequence of galaxy classes still in use today, to the equally famous and successful Galaxy Zoo project that employs citizen scientists around the world to visually classify galaxy images (Lintott et al. 2008). Now, with continued advances in telescope technology that will yield sufficiently large data samples to formally qualify as ‘big data’, most notably represented by the recently launched Euclid mission and upcoming LSST survey, sophisticated machine learning computer algorithms must increasingly be relied upon for such a task. A key advantage, however, of a classical visual morpho-

² The observed degradation in image resolution for a given AGN host galaxy in our sample, as highlighted in the Appendix, when attempting to probe the same rest-frame wavelength by using mosaic images exposed at increasingly longer observed wavelengths, led us to conclude that no information was lost, or final conclusions altered, by foregoing their inclusion in our analysis. In other words, it was clear that by utilizing only the F150W-band mosaic, that we were always choosing the best imagery at hand to constrain galaxy morphology.

logical analysis of a humanly manageable galaxy sample, is that it is robust against the inevitable sources of uncertainty introduced by such automated computer algorithms. These algorithms are sufficient for constraining generalized properties, but often fail to consider the nuanced features of individual galaxies that must not be ignored if one is to hope to achieve a complete understanding of the physical phenomena leading to their structures (Reza et al. 2021; Walmsley et al. 2002). Furthermore, the requirements for machine learning and citizen science, i.e., very large data samples and/or reliable training sets, are not yet available for the data we use in this work.

3.1. AGN Host Galaxy Morphology Analysis

In the present study, we exploit the robustness of the visual classification method to identify merger signatures in images of 289 AGN host galaxies in the form of a galaxy-wide disturbance or asymmetry (see Bignone et al. 2017 and references therein). The method chosen closely adheres to the visual classification procedure defined by Kocevski et al. (2015) (which represents a refinement to the set of visual classification rules initially defined in Kocevski et al. 2012). We then follow this procedure with a quantitative computer visual analysis in the form of an automated non-parametric measure of the asymmetry in each galaxy’s spatial pixel distribution using the *statmorph* software (Rodriguez-Gomez et al. 2019).

3.1.1. Visual Classification

Kocevski et al. (2015) present a straightforward procedure for classifying the optical appearance of a galaxy into the following categories: undisturbed disk, disturbed disk, spheroid, point source, irregular, or galaxy merger. To streamline the results of our analysis, we classify as “disturbed” all galaxies identified as irregularly shaped; an obvious merger, such as a close pair with two visible nuclei, or a classic ‘trainwreck’ appearance; as well as an asymmetric disk. Likewise, all point sources, spheroids, and apparently symmetric disks were classified as “undisturbed.” We also chose to refine the “disturbed disk” category into “strongly” and “mildly” disturbed subcategories, as we observed significant numbers of both types in our trials. Finally, we classified the small number of apparently fully edge-on disk galaxies as “undisturbed”, under the presumption that a galaxy-wide disturbance would manifest itself in three dimensions and therefore be observable from all disk inclination angles relative to the observer.

3.1.2. Computer Vision

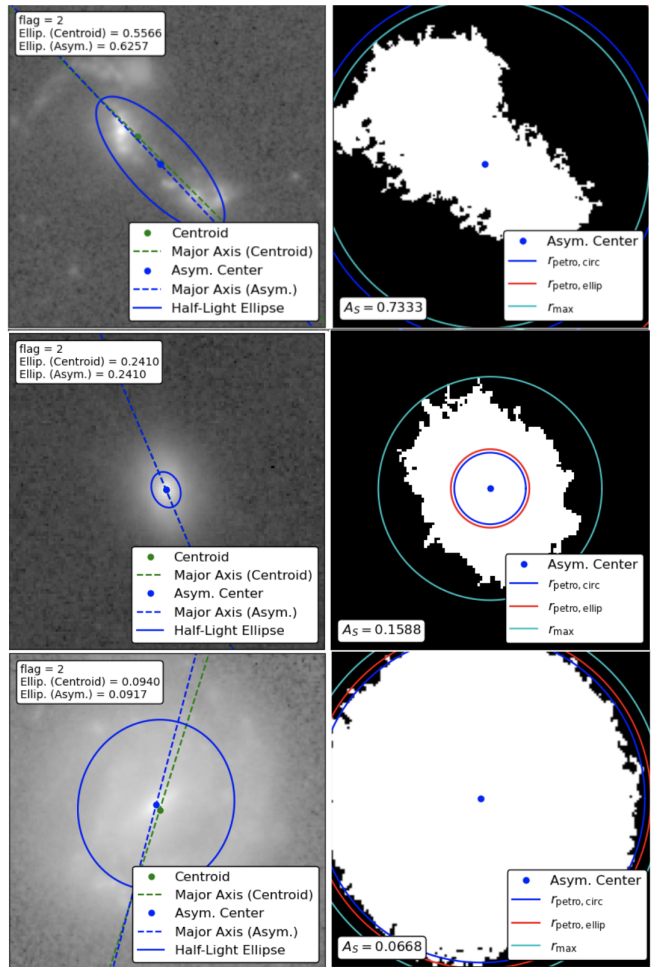


Figure 3. Examples of figure output from *statmorph* showing strongly asymmetric/disturbed (top, $A_s > 0.2$), mildly asymmetric/disturbed (middle, $0.1 < A_s < 0.2$), and symmetric/undisturbed (bottom, $A_s < 0.1$). The galaxy image is shown along the left column, and along the right column, the binary detection mask (segmentation map) used to calculate the shape asymmetry (A_s) parameter utilized in this study. The measurement is performed within the circular aperture set by r_{max} , defined by Rodriguez-Gomez et al. (2019) as the distance between the point that minimizes the standard asymmetry (A) and the most distant pixel that belongs to the detection mask (which differs slightly from the r_{max} value originally defined in Pawlik et al. 2016, who introduce A_s). The elliptical Petrosian aperture, centered on the point in the galaxy image that minimizes A , is used to calculate the sky background level in the galaxy image that sets the brightness threshold for the binary detection mask.

While visual classification tasks performed by a human have proven to be very accurate for many types of analyses (Brinchmann et al. 1998; Bundy et al. 2005; Kampczyk et al. 2007; Darg et al. 2010; Treister et al. 2012; Kartaltepe et al. 2015; Walmsley et al. 2002), by definition they are subject to ‘human

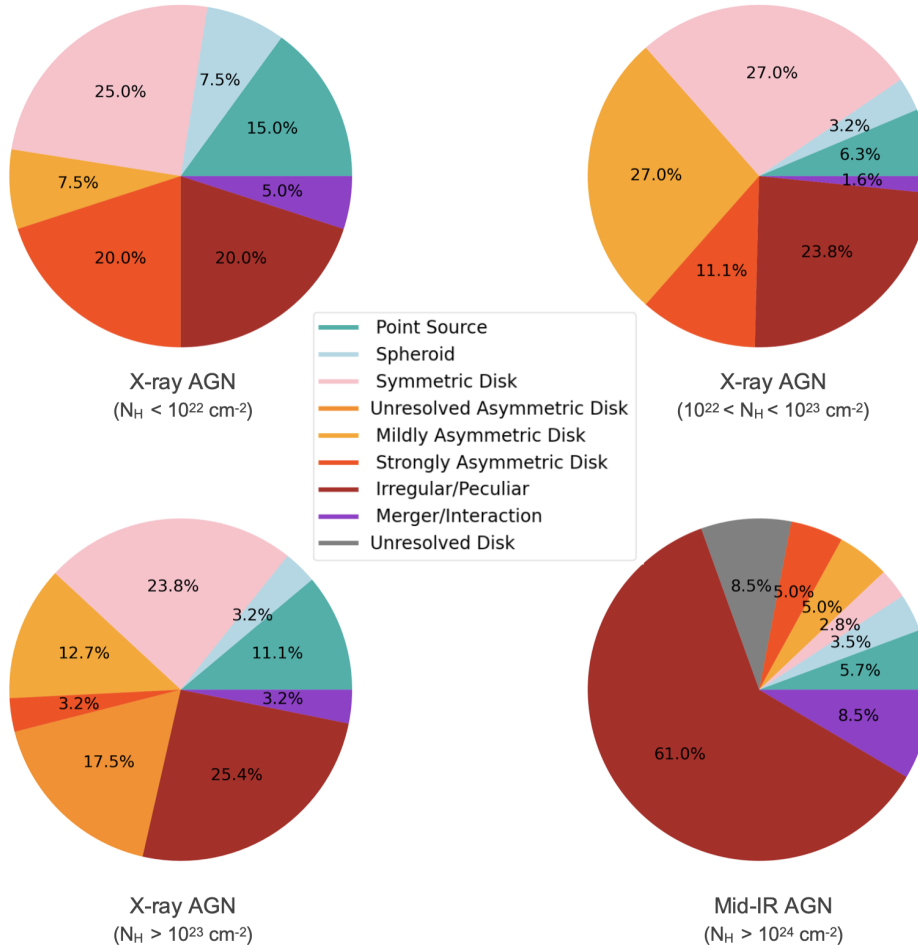


Figure 4. The results of the visual classification of the morphologies of the 289 AGN host galaxies in our sample, showing the percentage that are undisturbed (‘point source’, ‘spheroid’, and ‘disk’) and disturbed (‘merger’, ‘irregular’, and ‘disturbed disk’). Upper left: Least obscured X-ray AGN ($N_H < 10^{22} \text{ cm}^{-2}$). Upper-right: Moderately obscured X-ray AGN ($10^{22} < N_H < 10^{23} \text{ cm}^{-2}$). Lower-left: Heavily obscured X-ray AGN ($N_H > 10^{23} \text{ cm}^{-2}$). Note that the orange slice in this plot that represents ‘unresolved asymmetric disk’ (17.5%) marks cases where the galaxy image resolution was sufficient to visually detect an asymmetry, but not fine enough (or the galaxy size large enough) to distinguish between a mild and strong disturbance. Lower-right: presumed Compton-thick mid-IR-bright/X-ray-faint AGN.

error’ on account of oftentimes uncontrollable factors such as imperfect vision, and bias and differences in reasoning. In the context of our study, such error could have occurred in instances of modest image resolution or signal-to-noise, hidden evidence of weak galaxy disturbances such as faint tidal features; or if the strong inclination angle of a disk galaxy limited the view of mild spatial disturbances. Another important consideration in this context is the nonlinear response of the human eye to light intensity, that could have led to a mis-classification of truly disturbed galaxies as symmetric/undisturbed, e.g. in cases of high brightness contrast that would hide faint asymmetries/disturbances. Therefore, to systematically quantify the results of our visual analysis and catch such cases of subtle host disturbances that may have gone unnoticed or mis-categorized by the

human eye, we utilized the *statmorph* software package to perform an independent, computer visual check of the results. This software package was specifically chosen for its proven ability to detect faint merger signatures around the edges of galaxies (Rodríguez-Gomez et al. 2019).

The *statmorph* computer code reads a galaxy image and its associated weight map (the 1σ error image, also known as the ‘sigma image’ in *Galfit* and similar image analyses) to examine both the brightness and spatial distribution of its pixel values. It then calculates various measures of galaxy morphology, including the non-parametric measures of galaxy structure: asymmetry (A), clumpiness (S), concentration index (C), Gini index (G), and moment of light (M_{20}) (Lotz et al. 2004, Wu 1999, Bershady et al. 2000, Conselice et al. 2000,

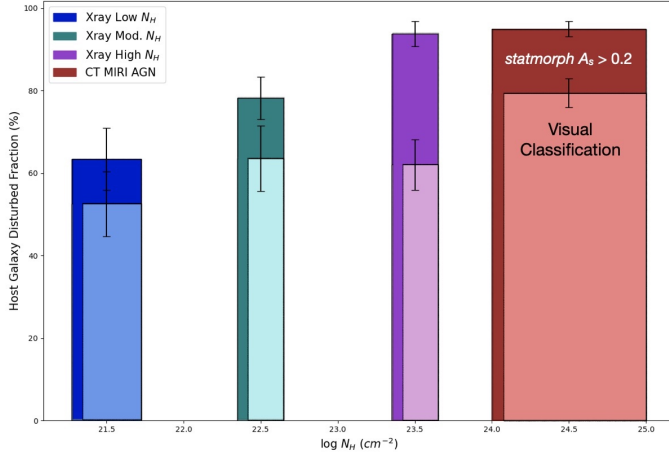


Figure 5. A comparison of the results of the *statmorph* $A_s \geq 0.2$ (dark colors) and visual (light colors, width artificially narrowed and offset for clarity) classification methods, showing the total percentage of AGN host galaxies presenting as strongly asymmetric/disturbed by the two independent analyses. It can be seen that the computer visual analysis identifies all of the strongly disturbed cases identified by the visual analysis, plus additional ones that evaded detection by the human eye. (Given that all/most of the *statmorph* $0.1 < A_s < 0.2$ mild asymmetry identifications were classified as undisturbed to the human eye, we show only the strongly disturbed *statmorph* results for the most conservative comparison to the visual classification results.) Bin placement and width (dark colors) correspond to the mean and standard deviation of the N_H bins for the X-ray test and control sub-samples; while the bin for the mid-IR-bright/X-ray-faint MIRI AGN does not reflect a physical measurement, but is artificially placed to represent the Compton-thick regime. Vertical error bars reflect the 1σ binomial standard deviation.

Schade et al. 1995, Abraham et al. 1994, Abraham et al. 1996, Isserstedt & Schindler 1986, Takamiya et al. 1999, Conselice et al. 2003). For our analysis, we focused on the *shape* asymmetry parameter, A_s , a relatively recent addition to the suite of galaxy morphological indicators introduced in Pawlik et al. (2016), explicitly to automate the recognition of galaxies with faint asymmetric tidal features suggestive of an ongoing or past merger. A_s is calculated in the same way as the standard asymmetry parameter, except the measurement is performed on the binary detection mask (segmentation map) of a galaxy rather than the galaxy image itself (see Pawlik et al. 2016 and Rodriguez-Gomez et al. 2019 for details). Therefore, while A considers asymmetries in both the spatial and brightness distributions of the pixel values in a galaxy image, A_s considers only those due to a spatial asymmetry, thereby isolating disturbances that can be attributed to a physically disruptive event such as a major merger, as

opposed to an internal galaxy sub-structure unrelated to merging activity that would qualify as a brightness asymmetry.

The binary detection mask utilized in the *statmorph* calculation of A_s is defined as the contiguous group of pixels brighter than 1σ above the mode of the pixel values in the background-subtracted, smoothed galaxy image, that includes the brightest pixel. Examples of the *statmorph* figure output showing the details of the A_s calculation are displayed in Figure 3. Pawlik et al. (2016) proved unequivocally that A_s far outperforms the classic A parameter in detecting low surface brightness features around the edges of a galaxy. In fact, until the addition of A_s to the suite of the classic CAS (concentration-asymmetry-clumpiness) and Gini coefficient model-independent measures of galaxy morphology, visual inspection was still considered a more accurate method to detect merger signatures than these parameters (see, e.g., Lotz et al. 2008, Darg et al. 2010, Treister et al. 2012).

For each of the 289 galaxies analyzed in our sample, we inspected and verified the automatically generated *statmorph* results to ensure proper source detection and aperture size and location. We identified and remedied instances where obvious foreground objects or image features/artefacts obviously not physically associated with the source being analyzed, were being included in the aperture used to calculate A_s . This was done by iteratively redefining the source aperture until such features were no longer erroneously being included in the A_s measurement. Therefore, the ultimate methodology we employed in our analysis of AGN host morphology was a synergistic union of human reasoning and computer vision.

3.2. Trial Design

Our analysis of AGN host galaxy morphology was conducted in two distinct trials (hereafter Trial 1 and Trial 2): the first considering only the X-ray-selected subset of AGN from Lyu et al. (2022) described in Section 2.1.1; and the second, those identified as mid-IR AGN without X-ray counterparts in Lyu et al. (2023), described in Section 2.1.2. To test the hypothesis of our study, we organized the trials in the following way: the X-ray AGN sample in Trial 1 was split into a test set of highly obscured sources ($N_H > 10^{23} \text{ cm}^{-2}$) and two control sets of unobscured-to-lightly obscured ($N_H < 10^{22} \text{ cm}^{-2}$) and moderately ($10^{22} < N_H < 10^{23} \text{ cm}^{-2}$) obscured sources, along the lines of the analysis in Kocevski et al. (2015), using the SED-modeled hydrogen absorbing column density parameter, N_H , as the measure of AGN obscuration. Trial 2 was designed to represent an

overlapping extension of Trial 1 in terms of an assumed increasing level of obscuration into the Compton-thick regime, as we require the mid-IR AGN sample to be undetected at X-ray wavelengths.

While the X-ray AGN sample size is not large enough to simultaneously match the test set of heavily obscured AGN to the moderately and lightly obscured control sets in narrow ranges of redshift (z), stellar mass (M_*), bolometric luminosity (L_{bol}), and intrinsic X-ray luminosity ($L_{x,int}$, X-ray 0.5 – 7 keV luminosity corrected for absorption), we found that dividing the sources into redshift bins of width unity between $z = 0$ and $z = 4$ had the effect of naturally binning on most of these other parameters. Where the primary redshift binning unavoidably led to a relatively coarse secondary bin on some of the other galaxy parameters tested, with ranges spanning 1 – 2 orders of magnitude in a given redshift bin, we repeated our analysis on each such parameter separately, to ensure no hidden biases in our final results. The chosen redshift bins, displayed in Figure 6, represent the maximum number of evenly spaced bins that allow for a statistically significant sample of galaxies in each, and are expected to be numerous enough to mitigate the effect of a redshift bias within a given bin. In other words, the probability of detecting morphological features in galaxies lying at similar redshifts should be roughly equal, given that any observed differences in their brightness and size would be due to intrinsic differences between the galaxies, and not to vastly different distances from the observer (see, e.g., Bamford et al. 2009). We also restricted our analysis to AGN in massive host galaxies with SED-derived (3D-HST photometry) stellar masses of $M_* > 10^9 M_\odot$ (Lyu et al. 2022), given the possibility that the dominant physical processes shaping the evolution of low-mass active galaxies may differ from those molding more massive ones; and that, in any case, the sample is likely incomplete and potentially biased for lower-mass hosts (Lyu et al. 2023).

What is evident in Figure 6 is the selection bias that plagues the X-ray detection of AGN, that low-luminosity, highly obscured AGN fall below the detection limits of the deepest X-ray surveys, leaving only the brightest sources to be selected at each redshift. The effect of this observational bias on the Trial 1 analysis is that the most obscured sources exhibit a median intrinsic X-ray luminosity significantly higher than the least obscured control set between $z=0$ and 1, and therefore these two subsets may not be meaningfully compared in this redshift bin. However, the moderately obscured control sample is well-matched in luminosity to both the highly obscured test set and least obscured control set

in each redshift bin, and therefore ‘bridges the gap’, so to speak, in the Trial 1 analysis.

For Trial 2, we split the mid-IR-bright/X-ray-faint AGN into the same redshift bins as for Trial 1, and repeated the same procedural analysis.

4. RESULTS

The results of the visual classification procedure for all trials are displayed in Figure 4, showing the percentage of AGN host galaxies with undisturbed (‘point source’, ‘spheroid’, and ‘disk’) and disturbed (‘merger’, ‘irregular’, and ‘disturbed disk’) morphologies. It can be seen that the morphology predominantly characterizing the disturbed X-ray AGN hosts is the ‘disturbed disk’ morphology, followed by irregular; the undisturbed fraction of the X-ray AGN hosts was likewise dominated by the (symmetric) disk morphology. The MIRI-detected sample, on the other hand, appears overwhelmingly irregular, with a higher fraction of obvious mergers.

In Figure 5, we compare the measured fractions of disturbed AGN host galaxies recovered by both the human and computer vision analyses. Unsurprisingly, the results of both largely corroborate one another, and it is clear that both methods reveal a correlation between disturbed host galaxy morphology and the level of AGN obscuration. The main difference found was that, in the visual classification, often what was qualitatively labeled as undisturbed, or a ‘mild’ galaxy asymmetry/disturbance to the human eye (a subcategory ‘learned’ after observing instances of significantly stronger disturbances), was classified by the *statmorph* A_s parameter as a ‘mild’ and ‘strong’ disturbance, respectively. Such undisturbed and mildly disturbed galaxies identified in the visual classification almost exclusively showed an A_s value between 0.1 – 0.2, and 0.2 – 0.3, respectively, ranges which define mild and strong asymmetries in *statmorph*. As a result, the computer vision analysis yields a higher fraction of disturbed AGN host galaxies than the visual classification procedure. We attribute this ultimately inconsequential difference between the two analysis methods to the numerical precision and objectivity of the shape asymmetry algorithm over human vision in classifying objects in an inherently unbiased way, and to its enhanced sensitivity to morphological asymmetries such as faint tidal features that might go unnoticed by the human eye. It proved particularly useful in the classification of the highly obscured systems lying at the highest redshifts, as these were sufficiently resolved to detect an asymmetry, but not enough for a fine visual distinction between a ‘mild’ and ‘strong’ (hidden) asymmetry (which may have led to a bias in the visual classification results where strong

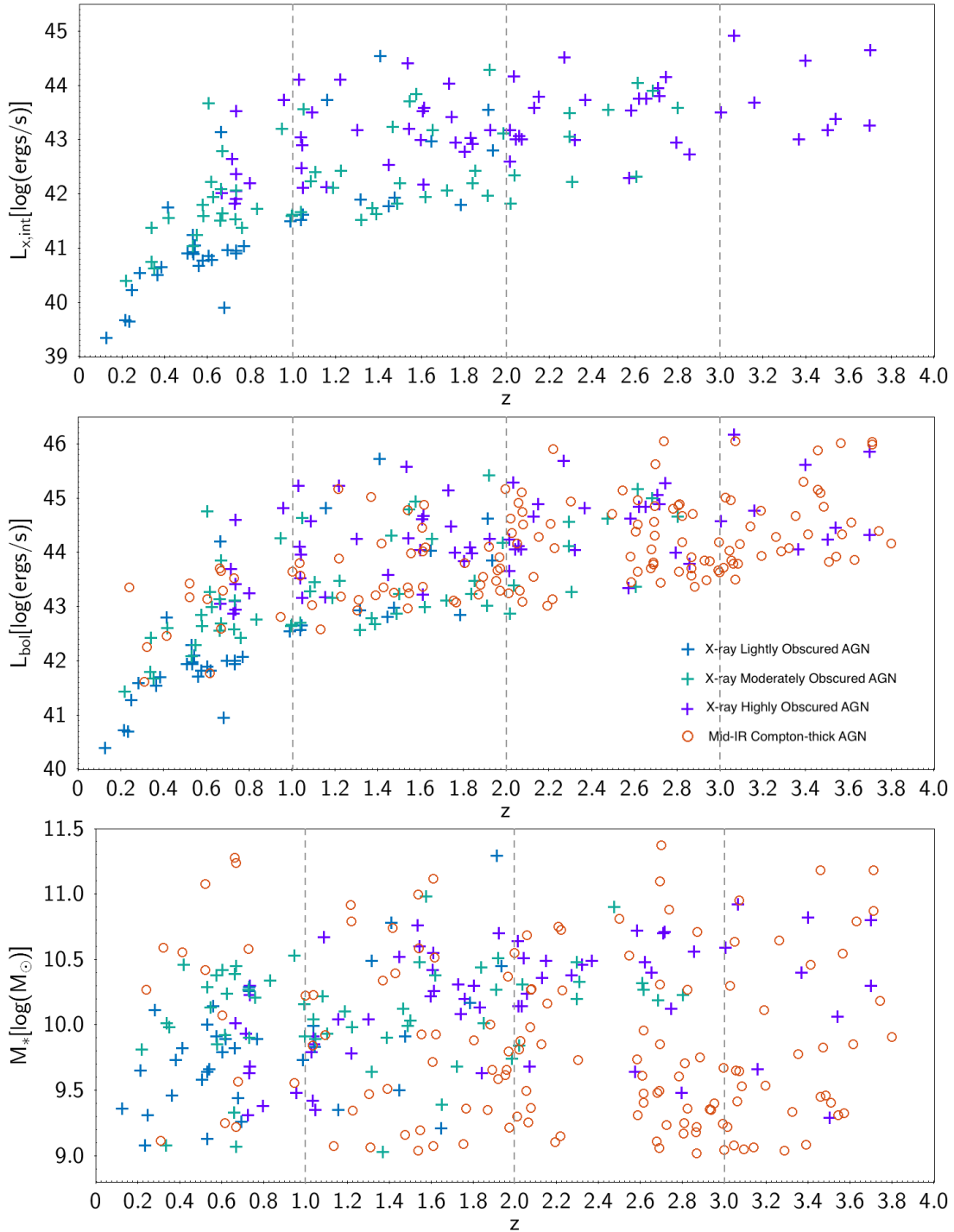


Figure 6. Top: X-ray intrinsic luminosities for the X-ray AGN sample as a function of redshift. Middle and bottom: X-ray and MIRI AGN sample M_* and L_{bol} as a function of redshift. Vertical gray lines mark the bounds of the four redshift bins in which the host galaxy morphologies of the AGN sample were separately analyzed and compared.

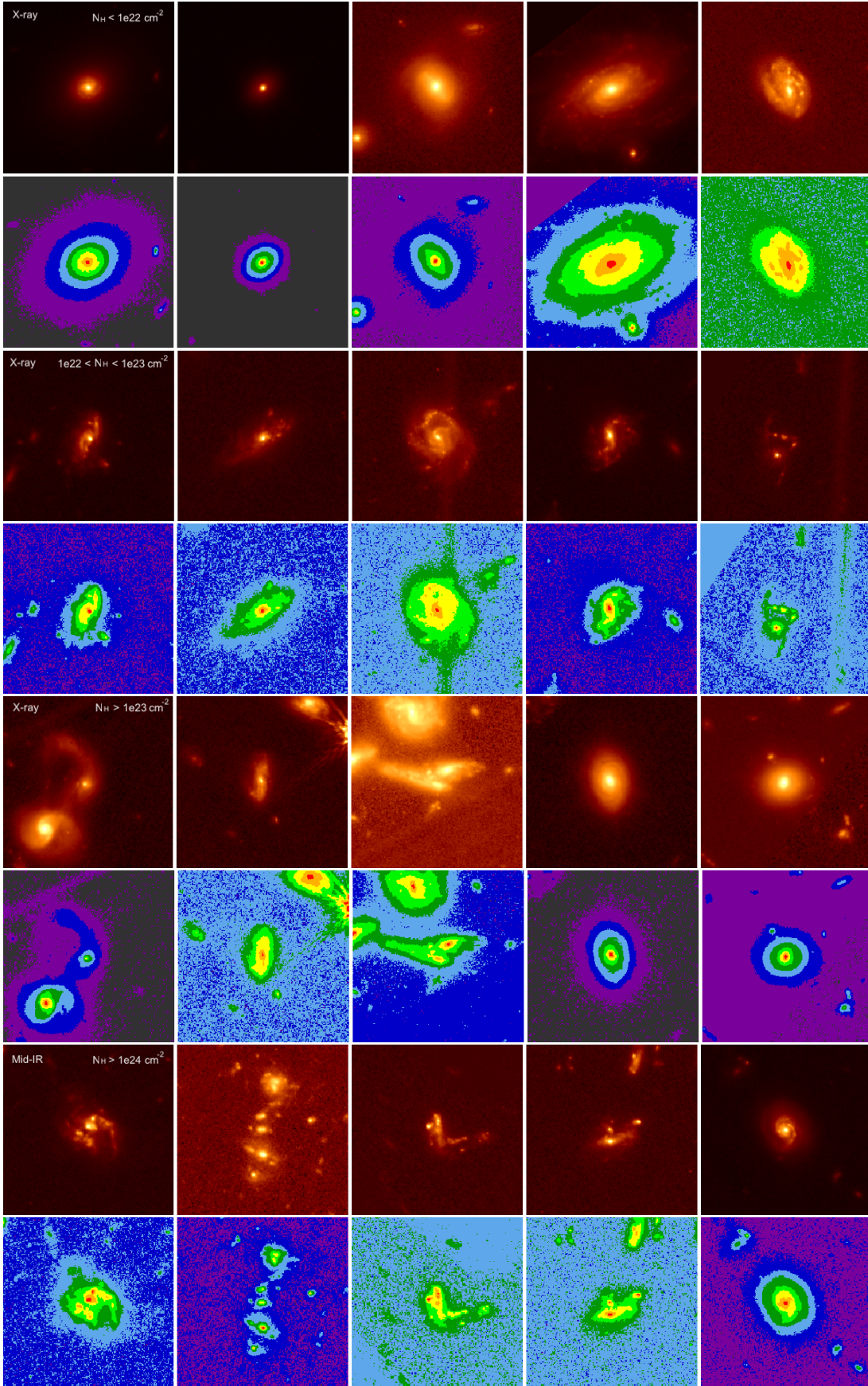


Figure 7. JADES v1 NIRCcam F150W mosaic image cutouts ($6'' \times 6''$) showing rest-optical AGN host galaxy emission of a representative sampling of the X-ray- and mid-IR-selected sources lying at $z = 1 - 2$. In these images, used in both the human and computer visual analyses of the present study, it can be seen that the galaxy morphologies range from visually undisturbed, symmetric shapes to highly asymmetric/disturbed. For the visual analysis task, the images were examined using a variety of SAOImage DS9 scales, stretches, and colors, to ensure the most accurate morphological classification, as demonstrated.

disturbances were more easily detected at low redshifts). We therefore adopt the *statmorph* analysis results as ‘final’, and all subsequent discussion in this paper is based on it.

We find that both the Trial 1 X-ray and Trial 2 mid-IR AGN samples significantly reside in host galaxies with disturbed morphologies at all redshifts sampled, and increasingly so towards higher redshift (in agreement with the general trend for galaxies to show a higher incidence of disturbances with increasing redshift (e.g., [Conselice et al. 2009](#)). The incidence of disturbance also increases with bolometric luminosity. The subset exhibiting the least amount of disturbance overall is the least obscured and least luminous X-ray AGN ($64 \pm 6.5\%$ strongly disturbed); while the subset with the highest fraction of strongly disturbed hosts is represented by the presumed most heavily obscured mid-IR-bright/X-ray faint AGN, whose hosts appear $95 \pm 4\%$ disturbed. The most obscured and luminous X-ray AGN appear just as disturbed at $94 \pm 6\%$, while the moderately obscured X-ray AGN show measurably less disturbance at $78 \pm 6\%$.

5. DISCUSSION

In both the visual classification and computer vision analyses of the JADES v1 rest-optical NIRC*am* images of X-ray- and mid-IR-identified AGN in GOODS-S/HUDF ([Lyu et al. 2022, 2023](#)), we find a strong correlation between the SED-inferred (or assumed, in the case of the mid-IR AGN sample) value of N_H , and the statistical fraction of host galaxies with a measurable galaxy-scale asymmetry/disturbance. This result is directly in line with the observed trend for $z < 2$ X-ray-luminous AGN analyzed in the same way in [Kocevski et al. \(2015\)](#), and directly extends their analysis out to $z \sim 4$. Like the authors of that study, we compare a test set of heavily obscured X-ray AGN to moderately obscured and unobscured-to-lightly obscured control counterparts, allowing us to isolate the effect of obscuration on AGN host galaxy morphology. Furthermore, by complementing the X-ray AGN sample with a newly identified sample of MIRI-detected, obscured mid-IR-bright/X-ray-faint AGN, we were able to carry our analysis into the presumed Compton-thick regime and begin to test the evolutionary scenario for AGN put forth in [Kocevski et al. \(2015\)](#) to explain their findings. These authors suggest that the most obscured X-ray- and mid-IR-detected Seyfert systems occur relatively early in the lifetime of a major merger, and chronologically precede the less-obscured and fainter X-ray sources. One way to frame the outcomes of the distinct trials in which we separately examined the host galaxy morphologies of X-ray- and mid-IR-identified AGN, would indeed be to propose

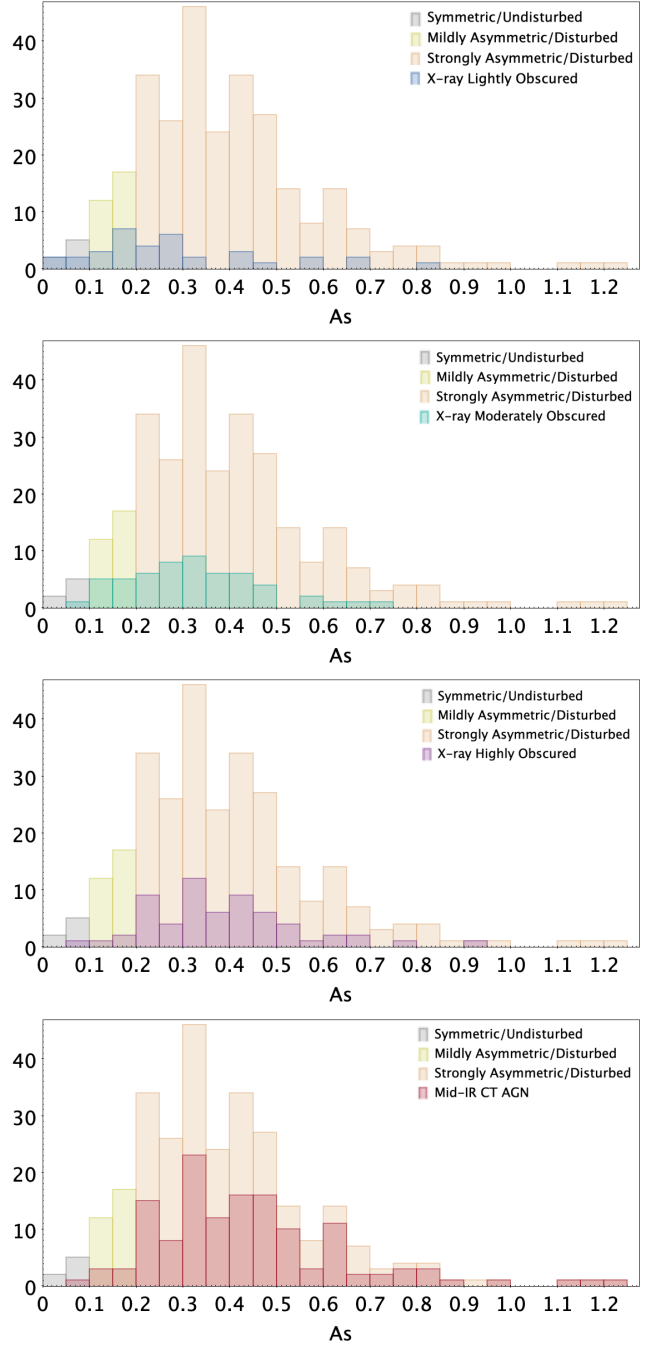


Figure 8. Histograms depicting the *statmorph* shape asymmetry parameter values for the full X-ray-plus-mid-IR AGN sample. From the top to the bottom of the column of figures, the values for the following subsets are separately overlaid in order to highlight the increasing fraction of disturbed hosts with N_H level: the X-ray unobscured/lightly obscured ($N_H < 10^{22} \text{ cm}^{-2}$), X-ray moderately obscured ($10^{22} < N_H < 10^{23} \text{ cm}^{-2}$), X-ray highly obscured ($N_H > 10^{23} \text{ cm}^{-2}$), and Compton-thick mid-IR AGN, respectively.

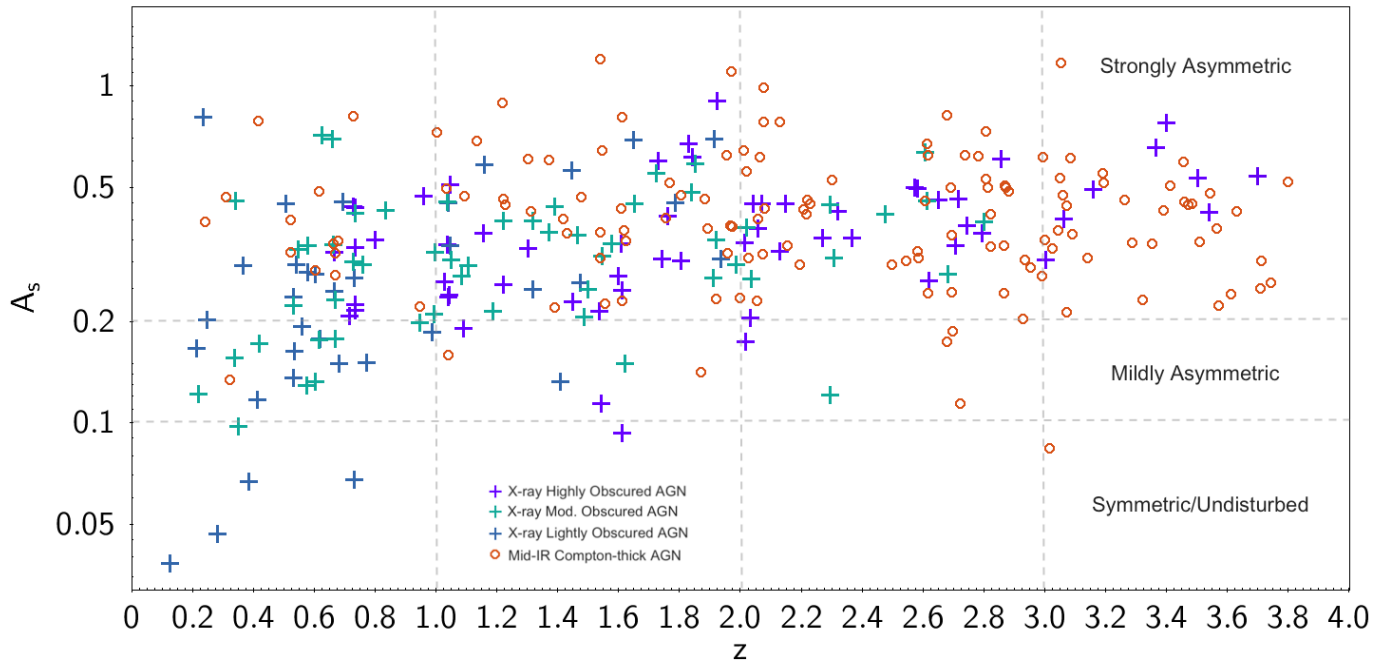


Figure 9. *statmorph* shape asymmetry (A_s) parameter values for the full AGN sample displayed as a function of redshift. A_s values between 0.1-0.2 represent mild asymmetry/disturbance, while values greater than 0.2 represent strong asymmetry/disturbance.

such a scenario. This appears supported by the merger simulations of Lotz et al. (2010), that disturbed host galaxy morphologies should be most noticeable both at the very start of a major merger, and also in the final stages. They also show that late-stage major merger remnants (~ 1 Gyr after coalescence) tend to appear as early-type spiral galaxies, which would suggest that our disturbed X-ray AGN sample, that is dominated by the disk morphology, may be major-merger remnants being ‘caught’ at a later stage than the largely irregular/train-wreck mid-IR AGN (Bignone et al. 2017).

The strength of our analysis lies in the experimental design of our trials, and the superior NIRCcam rest-optical imagery utilized. These points are expanded upon, below.

1) By partitioning a single and relatively complete sample of X-ray AGN that were detected using the same method and extracted from the same data set – and matched on numerous physical traits but exhibiting distinct levels of N_H obscuration – we were able to eliminate a maximum number of uncontrolled variables and observational biases that might otherwise skew the results of our analysis. Most importantly, this approach allowed us to test a model-predicted evolutionary scenario in which the obscured and less-obscured phases of AGN occur in chronological succession of one another. Had we compared a test set of AGN hosts to a control sample of non-active counterparts without distinc-

tion between the obscured and unobscured subsamples (see, e.g., Kocevski et al. 2012), we could easily have missed this connection. In other words, the experimental design of our trials was aimed at directly testing the narrowly focused scientific question of whether or not the obscured AGN phase is strongly associated with mergers, as opposed to measuring the fraction of active galaxies versus non-active galaxies associated with mergers (which is a worthwhile and necessary pursuit that fits into our broader scientific study, but is beyond the scope of the current paper).

2) The capabilities of JWST have allowed the measurement of detailed morphologies of AGN host galaxies in rest-optical imagery with high signal-to-noise and out to high redshift. In addition, the follow-up to our visual classification of AGN host morphologies with a computational analysis using the relatively new *statmorph* shape asymmetry parameter, was key in allowing us to circumvent the obstacles faced by previous authors: we observed firsthand how a non-negligible number of mildly asymmetric/disturbed disk galaxies in our sample could go unnoticed by the human eye and initially be classified as ‘undisturbed’ – only to discover in the results of the computer vision analysis that they are, in fact, significantly asymmetric. This can be attributed to the inherently unbiased nature of the *statmorph* A_s algorithm in its assignment of equal weights to all pixels in an input image belonging to a galaxy, using the binary

segmentation image of the galaxy, i.e. without consideration of the brightness variations amongst the pixels, as traditionally done with classic non-parametric morphology indicators. This translates to detecting asymmetries resulting purely from spatial/morphological disturbances, as opposed to an asymmetry in pixel brightness values, e.g. due to a galaxy sub-structure not caused by or related to physically disruptive merging activity. At the time of writing, to the extent of the authors’ knowledge, the present study represents the first to quantitatively tie ongoing or past merging activity to the obscured phases of AGN through the measure of AGN host galaxy spatial morphology.

Even if we were to take a conservative approach and entirely remove the *statmorph* computer vision analysis to use only visual classification, in keeping with all previous studies on the topic, our main result would still hold. In this case, we would effectively re-classify a significant number of the *statmorph*-detected-but-invisible “mildly disturbed” cases ‘back’ to the visually undisturbed category, still leaving the “strongly disturbed” cases that were observed using both the visual and computational methods, and that represent the bulk of the disturbed fraction.

5.1. Comparison to previous observational studies

We confirm and expand upon the main conclusion of Kocevski et al. (2015), that a majority of the heavily obscured X-ray AGN at sub-quasar luminosities are found in hosts with a measurable galaxy-scale spatial asymmetry/disturbance. We additionally observe that the overall fraction of AGN hosts exhibiting a disturbed morphology in rest-optical imagery grows in step with redshift in both the X-ray and mid-IR samples of our analysis, along with N_H and intrinsic X-ray luminosity in the X-ray sample, and bolometric luminosity in the mid-IR-bright/X-ray-faint subset. The hosts of the most obscured X-ray AGN ($N_H > 10^{23} \text{ cm}^{-2}$), and the Compton-thick mid-IR-bright/X-ray-faint MIRI AGN, represent the most disturbed subsets of the entire sample showing $\sim 94\%$ and $\sim 95\%$ strong disturbance, respectively, and rank consistently among the most disturbed in all data bins considered in our trials with fixed redshift, stellar mass, and intrinsic X-ray luminosity, between 85% and 100% percent disturbed. The moderately obscured ($10^{22} < N_H < 10^{23} \text{ cm}^{-2}$) X-ray AGN show a slightly smaller strongly disturbed host fraction of 78%, while the least/unobscured ($N_H < 10^{22} \text{ cm}^{-2}$) show the lowest of the entire sample at $\sim 64\%$.

In Kocevski et al. (2015), a picture of AGN evolution is suggested that would unify the results of their analysis through a chronological ordering of the obscured and

unobscured X-ray AGN phases considered in their study. It proposes that the X-ray AGN exhibiting the highest (sub-quasar) $L_{x,int}$ and N_H values, and level of galaxy-scale morphological disturbance, appear relatively early in the lifetime of a major merger, before a fully enshrouding dusty torus begins to block all X-ray (and optical) emission from the accretion disk. This heavily obscured phase, during which the AGN may only be detected via significant warm and hot dust re-emission in the mid-IR, and marking the presumed period of significant black hole growth, would then transition to the briefly visible quasar phase as the increase in radiative power from the nucleus reactively “blows out” the obscuring dust and gas. This would ultimately lead to the presentation of a naked, unobscured X-ray AGN with a steadily diminishing X-ray luminosity and increasingly more ordered and relaxed morphology. This observed strong correlation of host galaxy morphological disturbance with N_H level in our own analysis of obscured and unobscured/lightly obscured X-ray AGN, taken together with the trends in the luminosities of each of the X-ray and mid-IR AGN subsamples discussed in Section 4, appears to fit into the same evolutionary picture.

5.2. Comparison to models and merger simulations

The AGN-fueling model put forth in Hopkins et al. (2014) predicts that quasars are predominantly merger-fueled, as supported by numerous empirical studies (e.g. Hopkins & Hernquist 2006, Glikman et al. 2015, Assef et al. 2016, Fan et al. 2016, Treister et al. 2012), while stochastic processes dominate SMBH growth in low-to-moderate luminosity AGN with $M_{BH} < 10^7 M_\odot$ (see Treister et al. 2012). However, given the expectation that the bulk of the faint/obscured AGN population remains largely hidden below the detection limits of even the deepest X-ray surveys, there is the possibility that this model has been significantly under-tested in the mass and luminosity regime of Seyfert galaxies. The newly uncovered set of obscured MIRI AGN added to our comprehensive X-ray sample from Lyu et al. (2022), places us at a unique vantage point to test this very theory. Furthermore, it is also possible, as Hopkins et al. (2014) directly address, that any significant evidence of mergers that may exist in the low- and intermediate-luminosity AGN population has simply gone undetected due to the inherent faintness and short lifetime of merger signatures such as tidal tails. While the results of our study agree with theirs superficially in the prediction of a rise in merger-driven SMBH accretion with redshift and luminosity, reflecting the expectation of a cosmological merger rate rapidly increasing with redshift, we observe this trend in the realm of AGN luminosities and

SED-inferred black hole masses far lower than predicted by Hopkins et al. (2014). Therefore, we must consider that, while this model is physically sound and has been proven to accurately predict the dominant fueling mechanism of the brightest and most massive (i.e. most easily detected) AGN (see, e.g. Treister et al. 2012), that its predictions in the Seyfert regime need to be improved.

5.2.1. *On the predominance of disk morphologies*

We also find, like Kocevski et al. (2015), that the majority of the X-ray AGN hosts in our study are disks, as opposed to the point sources or spheroids that might be expected to emerge from a merger. In fact, their finding of a high disk fraction amongst obscured AGN hosts to a luminosity $10\times$ brighter than predicted by Hopkins & Hernquist (2006), prompted those authors to revise the merger-induced fueling component of their model in Hopkins et al. (2014) to better reflect such observations. One of the major claims of Hopkins et al. (2014), based on both their model predictions and observations they cite in support of them, is that an AGN host with a disk morphology should be taken as evidence of being ‘stochastically fueled’, that one would expect a ‘merger-fueled’ AGN to appear as bulge-dominated in a post-merger phase. The implication of this assumption on their models for AGN fueling is that at sub-quasar luminosities and at $M_{BH} < 10^7 M_{\odot}$, SMBH growth should be dominated by secular, passive processes, at all redshifts, and by merger-induced growth at quasar luminosities and $M_{BH} > 10^7 M_{\odot}$. Our findings are in direct disagreement with this model, which would be alarming had Hopkins et al. (2014) not explicitly highlighted the tremendous difficulty of detecting inherently faint tidal signatures around a galaxy of a recent, or even ongoing merger, even in local systems, compounded by surface brightness dimming for more distant galaxies (see, e.g., Lotz et al. 2008). As a result of this, there is a record in the literature of major mis-classifications of such galaxies as “relaxed” using HST imagery, which was primarily and necessarily relied upon before the advent of JWST and its superior sensitivity and resolution (see, e.g. Hopkins et al. 2009b, Lotz et al. 2004).

It is also important to consider that Hopkins et al. (2009) thoroughly demonstrate in simulations of mergers of varying mass ratios, gas content, and orbital parameters, that it is quite common for disks to survive or reform following a merger, based on simple laws of gravitational physics and independent of the details of ISM gas physics or feedback processes. Darg et al. (2010) take their analysis further and provide empirical evidence that the timescale of detectability for mergers involving spiral galaxies is longer than those involving el-

lipticals, as theoretically predicted by Lotz et al. (2008). Furthermore, the merger simulation study of Bignone et al. (2017) that uses Illustris TNG mock galaxy data to constrain the non-parametric morphologies of mergers, finds that rotationally supported gas-rich structures can form from residual angular momentum after the final coalescence of the merging galaxies, despite the Illustris galaxy formation model including feedback from quasar- and radio-mode AGN, and stellar supernovae; this finding is also supported by Robertson et al. (2006) and Snyder et al. (2015). Finally, the merger simulations of Lotz et al. (2008) show that the remnants of equal-mass, gas-rich isolated mergers appear disk-like when observed at $t > 1$ Gyr after the final coalescence. Therefore, the fact that the members of the X-ray AGN sample studied here lie mostly in disk morphologies, as opposed to the spheroidal, bulge-dominated systems historically expected to emerge from a merger, should not be as surprising as Hopkins et al. (2014) would indicate; it cannot be used as direct evidence against their formation in a past merger (Hopkins & Hernquist 2006). It could still be the case, however, that AGN residing in fully relaxed or very mildly disturbed disks represent a phase sufficiently long after a potential past merger that their primary fueling mechanism has transitioned to more passive processes.

5.2.2. *Redshift-dependent disturbance*

Several features of our analysis appear to support the model-predicted increase in merger-driven accretion with redshift, if we can safely assume that merging activity is correlated with obscuration and AGN bolometric luminosity. In other words, we observe an increase in the level of AGN host galaxy disturbance and level of N_H obscuration – which we assume to be merger-driven – with redshift, which also traces an increase in L_{bol} in our sample. We do not observe many unobscured/lightly obscured X-ray AGN at $z > 2$, most in our sample reside at $z < 1$; conversely, very few of the highly obscured and most disturbed AGN lie at the lowest redshifts. This trend reflects the X-ray survey detection limit where we miss the faintest high- N_H AGN at high redshift, but it is also not clear if we can even expect a significant number of obscured systems below the detection limit at these high redshifts (see, e.g. Hickox & Alexander 2018). In other words, we may be witnessing a true redshift-dependence of the AGN level of obscuration and luminosity tied to an increasing level

of host galaxy disturbance, and not merely an artificial result from selection bias.³

Finally, of note is that in the redshift bin of our analysis sampling AGN at $z = 1 - 2$, all subsets appear with a high number of disturbed hosts, including the low- N_H , unobscured-to-lightly-obscured X-ray AGN. While we observe that these systems are found in nearly equal numbers of disturbed and undisturbed hosts at $z < 1$, in agreement with numerous other studies and the expectations of the AGN fueling model of Hopkins & Hernquist (2006), the fraction of disturbed hosts among this subset jumps from 64% at $z < 1$ to 91% between $z = 1 - 2$, in the same realm as their more obscured counterparts at these redshifts – though we caution that this data bin may be skewed by small-number statistics. Even so, we observe the fraction of mildly disturbed unobscured hosts increases from 40% at $z < 1$ to 72% at $z > 1$, which may be significant. Likewise, the disturbed host fraction of the moderately obscured counterparts sharply rises from 65% to a maximum of 95% between $z = 1 - 2$, with a constant ratio of mild-to-strong disturbance. This observed uptick in the disturbed host fraction in our sample at $z \sim 1$ matches the findings of Treister et al. (2012), who concluded that the dominant source of SMBH growth appears to transition from secular processes to mergers at this redshift, based on an analysis of ten archival surveys of moderate-luminosity AGN at $z < 3$.

6. OUTSTANDING QUESTIONS

6.1. Major, minor, or accumulated mini mergers?

While it is accepted in the literature that galaxy disturbances measured using conventional non-parametric morphology indicators are to be interpreted as merger signatures, the asymmetry measurements alone cannot generally be used to determine whether the disturbance is caused by a major or minor merger, or a steady accumulation of mini mergers. The distinction is important in the context of our study, given the assumption that only gas-rich major mergers can significantly contribute to the growth of SMBHs. Lotz et al. (2008)

and Bignone et al. (2017) correlate key non-parametric morphology measures with the recent merger history of galaxies to show that the $Gini - M_{20}$ criterion is effective at identifying both major and minor mergers over a significant lifetime of the merger. However, it is most complete and effective in the pre-coalescence phase while a double nucleus is visible, given the nature of the measurement. These authors also show that the classic asymmetry (A) parameter can be used to loosely distinguish major from minor mergers where two nuclei are still visible. Even so, Bignone et al. (2017) emphasize that these metrics can be quite incomplete in their identification of mergers, especially in the post-coalescence phase. In addition, Pawlik et al. (2016) showed that A_s is much more sensitive to faint tidal signatures indicative of a merger than A , which was the very motivation for their invention of A_s . Furthermore, the simulations in Bignone et al. (2017) showed that A classifies as disturbed all galaxies with stellar masses less than $10^{10.5} M_{sun}$, independent of a merger event. Therefore, we also consider this parameter to be unreliable in identifying merger remnants. As such, we are not able to show with the *statmorph* non-parametric measures alone if the AGN hosts in our sample are likely to be the remnants of major or minor mergers, given that only a small handful of our entire sample meet the double-nucleus criterion. However, the presentation of a significant number of strongly disturbed disk morphologies in the X-ray sample suggests they could likely be the remnants of the gas-rich mergers that are believed to fuel SMBH in the Universe, as 1) the presence of a disk indicates the presence of gas; 2) merger simulations (Lotz et al. 2008; Bignone et al. 2017) consistently show that spiral morphologies can reform after major gas-rich mergers and appear as disturbed disks to ~ 1 Gyr post-coalescence; and 3) at any given snapshot along the cosmic timeline during which merging galaxies are expected to occur in the Universe, we are more likely to observe the remnants of major mergers than minor mergers, given the significantly longer timescale of observability (~ 2 Gyr) of the former (Lotz et al. 2010; Bignone et al. 2017). However, the simulations of Lotz et al. (2008, 2010) did not include the effects of AGN feedback, and therefore it is not clear if a gaseous disk could survive or reform post-major-merger in more realistic conditions. They also did not consider mergers involving mixed-morphologies, e.g. a disk merging with a spheroid.

The Illustris merger simulations of Bottrell et al. (2023) find that so-called mini mergers ($0.01 \leq \mu < 0.1$) are expected to occur significantly more frequently than minor and major mergers, and therefore may represent a significant, overlooked cause of galaxy morphological

³ However, the explanation for why we do not observe luminous unobscured AGN in our sample is less clear, but may very well reflect the rarity of catching a snapshot of the relatively short-lived optical quasar phase ($\sim 10^7$ years), in comparison to the longer pre- and post-quasar phases (see Hopkins & Hernquist 2006 and references therein). There is also the expectation of a decreasing number of massive gas-rich mergers with decreasing redshift and associated predominance of dry mergers at $z < \sim 1.5$ (Treister et al. 2012), reflecting an antihierarchical black hole mass growth in which quasar peak luminosities and (final black hole masses) markedly decline at $z < 2$ (Hopkins & Hernquist 2006).

disturbance. While the simulations show that individual mini mergers are not likely to induce a significant observable disturbance, they reveal that the integrated (classic *A*, light-weighted) asymmetry due to mini mergers over $0.01 \leq z \leq 0.7$ constitutes 70% of the asymmetric structure in the mergers of their study. They therefore suggest that the aggregation of asymmetry enhancements by a series of mini merger events for a given galaxy may be driving the build-up of light asymmetry and lopsidedness in galaxies, as opposed to major or minor mergers. However, their study examined only TNG50 star-forming galaxies and adopted the classic asymmetry parameter as the measure of galaxy disturbance, while we consider *active* galaxies and utilize the *shape* asymmetry parameter that ignores asymmetries in the galaxy surface brightness distribution. As a result, it is not immediately clear if the results of their study have direct implications for ours.

7. CONCLUSION

This study directly builds upon and reaffirms the results of Kocevski et al. (2015), who compare the morphologies of a significant number of obscured X-ray-selected AGN to their unobscured counterparts, in an attempt to test the suspected connection between obscuration and merger activity. Like Kocevski et al. (2015), we split an X-ray sample of AGN into ‘test’ highly obscured and ‘control’ moderately and lightly obscured subsets, and match them on stellar mass, bolometric luminosity, and redshift. However, we were able to extend the analysis into the Compton-thick regime using a newly obtained sample of mid-IR-bright/X-ray-faint JWST/MIRI AGN; and also into the high-redshift regime to $z \sim 4$, using highly resolved, high-signal-to-noise JWST/NIRCam rest-optical imagery from the JADES v1 data release. We find a significant correlation between host galaxy disturbance and level of AGN obscuration amongst a complete, multi-wavelength sample of obscured Seyfert AGN at $z = 0 - 4$, using both a qualitative visual classification and quantitative measure of the shape asymmetry of each galaxy in question. From the observed pattern of disturbances, we conclude that mergers are common amongst the obscured AGN population, and therefore that the obscured AGN phase may mark a period of significant supermassive black hole (SMBH) growth – in direct tension with the leading model on AGN fueling mechanisms (Hopkins et al. 2014). Specifically, there is the possibility that the merger-fueled AGN phase predicted by Hopkins et al. (2014) to exclusively reside in the quasar regime, extends to the significantly lower Seyfert luminosities and black hole masses sampled here. This may be the re-

sult of their model missing a significant fraction of faint obscured AGN that are now ‘coming to light’, and that may represent relics of quasar activity in the distant past (so-called ‘dead quasars’). If such systems were in fact born from mergers and not other, more passive processes – as might be indicated by the observation that the Seyfert luminosity function smoothly joins onto the quasar luminosity function (Hao et al. 2005) – they could be expected to be sporadically revived by such secular processes, leading to their presentation as ‘non-mergers’.

This theory appears to be supported by McAlpine et al. (2020), a study that utilizes the cosmological hydrodynamical EAGLE simulation to investigate the degree to which black hole (BH) activity is enhanced during the period of a major merger. This study finds that the galaxies embodying the most optimal conditions for triggering an AGN via a merger have the relatively low stellar masses, black hole masses, and luminosities typical of the AGN in our sample. The second key discovery of their study is that 50-75% of major-merger-triggered BH activity occurs in post-merger systems, *after* the two galaxies have coalesced. This implies that the majority of observational merger studies, which focus on the earliest stages of a merger, may have missed a significant fraction of the peak of BH growth in their samples, and mistakenly classified the post-merger remnants as isolated, non-merger AGN.

The strength of our conclusion not only lies in the corroboration of the results of Kocevski et al. (2015) and expansion to higher redshifts and levels of AGN obscuration, but also in the agreement with the various merger simulations discussed. In Paper II, we will expand upon the analysis of this paper with supplementary data from the literature to further investigate if the Seyfert population sampled may evolve according to a lower-luminosity, lower-mass extension of the accepted quasar evolution models put forth in Hopkins & Hernquist (2006), Hopkins et al. (2009), and Hopkins et al. (2014) as the data would suggest.

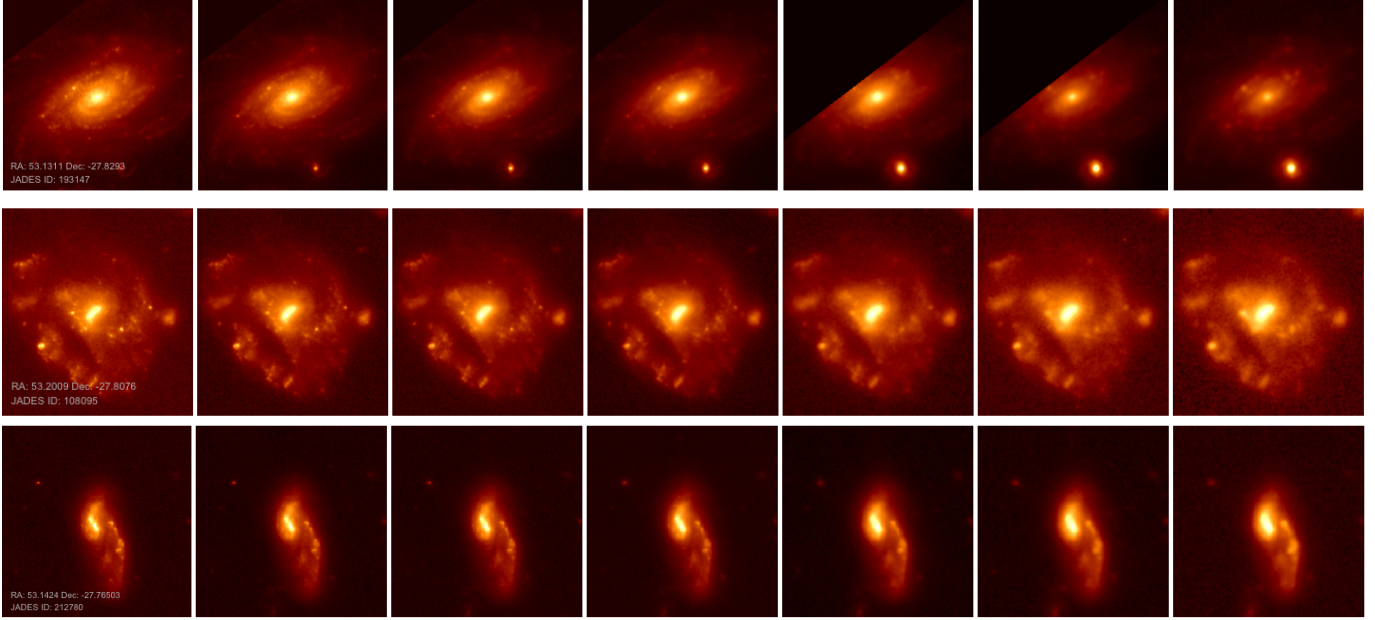


Figure 10. JADES v1 mosaic image cutouts of lightly obscured ($N_H < 10^{22} \text{cm}^{-2}$) X-ray-selected AGN at $0 < z < 1$ (Lyu et al. 2022) in the following NIRCcam bands (left to right): F090W, F115W, F150W, F200W, F277W, F356W, F444W.

APPENDIX

Here we show the JADES v1 mosaic NIRCcam cutout images of a randomly chosen and representative selection of the AGN in our sample at the effective wavelengths available (listed in the image captions), to demonstrate the progressive resolution degradation inevitably caused by an increasing PSF size towards longer wavelengths. This instrumental effect motivated our decision to include only the F150W mosaic imagery in our analysis, as it represents the mosaic at/near peak NIRCcam resolution and sensitivity that also maximizes the coverage of our AGN sample in the GOODS-S field. We observed, after repeatedly visually examining a statistically significant number of images of the AGN host galaxies in a number of trials, that no information would be gained or lost, or conclusions altered, by measuring the AGN host galaxy morphology at a constant rest-frame wavelength, requiring our analysis procedure to be repeated using mosaic image cutouts at a range of observed wavelengths other than (longward of) F150W. It can be witnessed here in all images shown, that the morphological identification of each galaxy as measured in the F150W image as symmetric/undisturbed or asymmetric/disturbed, remains unchanged in the images exposed at other wavelengths; all galaxy images exposed at wavelengths longward of F150W appear identical to the galaxy image at F150W, except at poorer resolution. We also note a similar observance of the images taken at wavelengths shortward of F150W: while they appear equally or slightly more resolved than the F150W image (but noisier), the galaxy morphology appears identical and therefore no new information would be gleaned from inclusion of these images in our analysis.

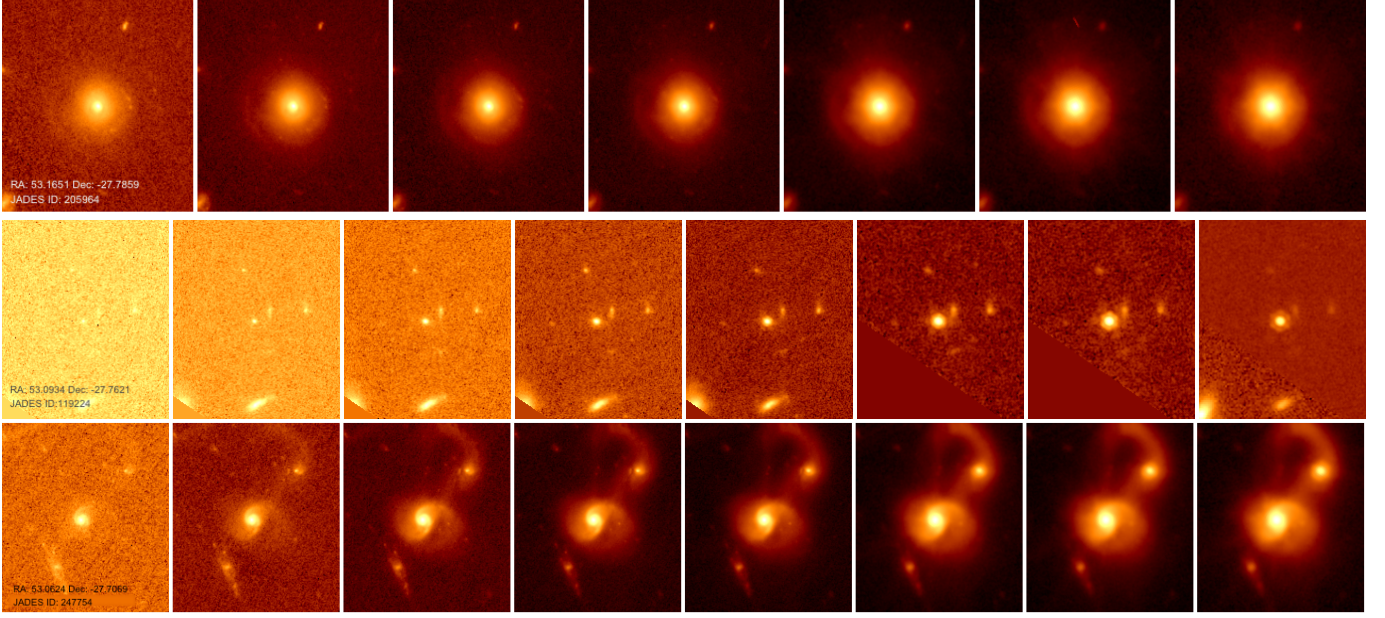


Figure 11. JADES v1 mosaic image cutouts of lightly obscured ($N_H < 10^{22} \text{ cm}^{-2}$) X-ray-selected AGN at $1 < z < 2$ (Lyu et al. 2022) in the following NIRCcam bands: (Top) F090W, F115W, F150W, F200W, F277W, F356W, F444W; (Middle, Bottom) F070W, F090W, F115W, F150W, F200W, F277W, F356W, F444W

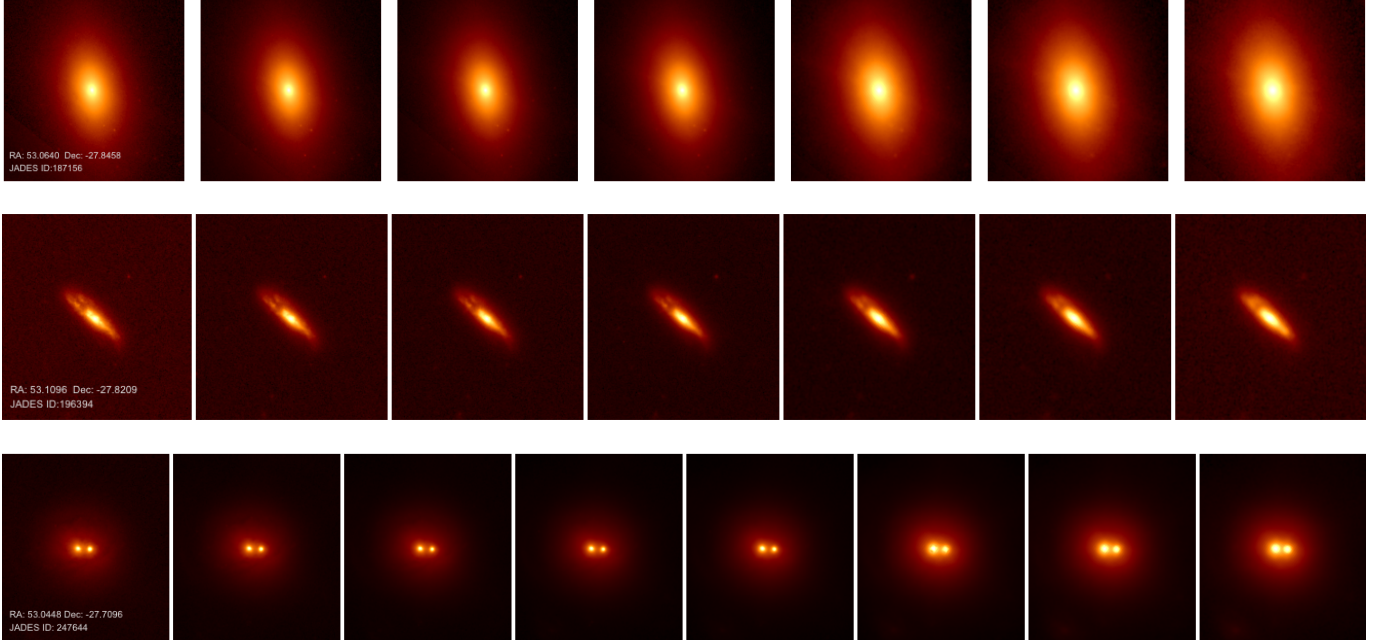


Figure 12. JADES v1 mosaic image cutouts of moderately obscured ($10^{22} < N_H < 10^{23} \text{ cm}^{-2}$) X-ray-selected AGN at $0 < z < 1$ (Lyu et al. 2022) in the following NIRCcam bands: (Top, Middle) F090W, F115W, F150W, F200W, F277W, F356W, F444W; (Bottom) F070W, F090W, F115W, F150W, F200W, F277W, F356W, F444W

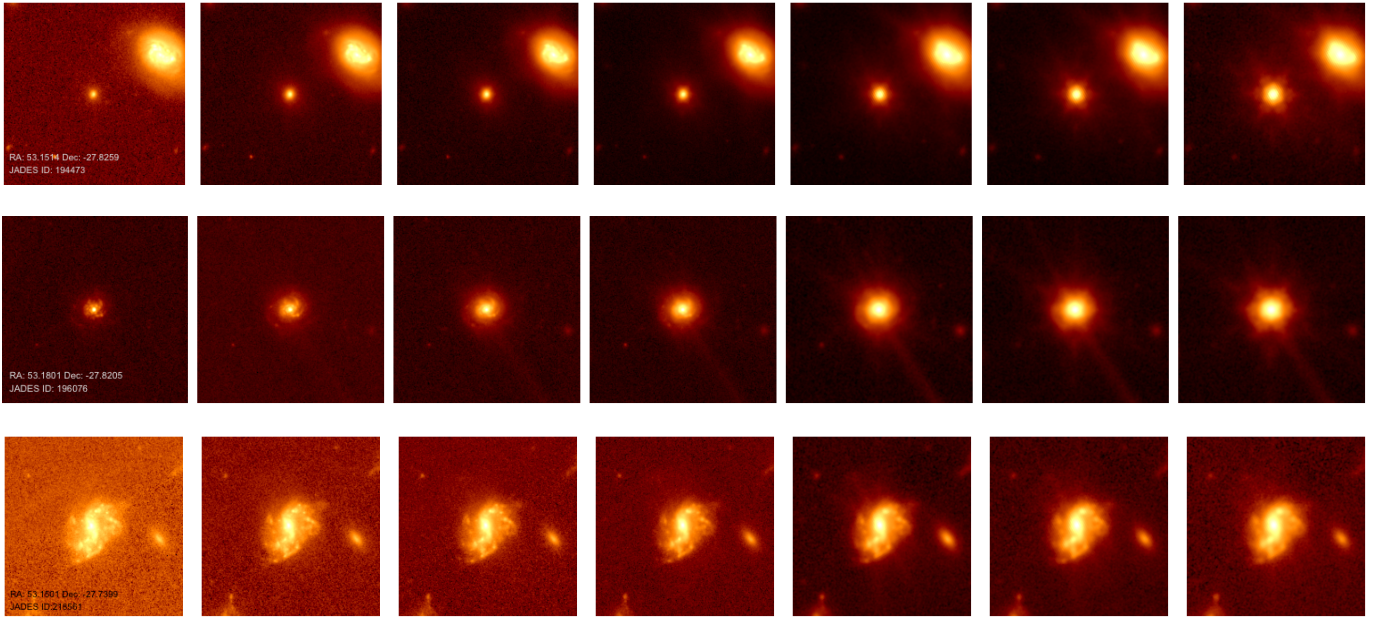


Figure 13. JADES v1 mosaic image cutouts of moderately obscured ($10^{22} < N_H < 10^{23} \text{ cm}^{-2}$) X-ray-selected AGN at $1 < z < 2$ (Lyu et al. 2022) in the following NIRCcam bands: F090W, F115W, F150W, F200W, F277W, F356W, F444W

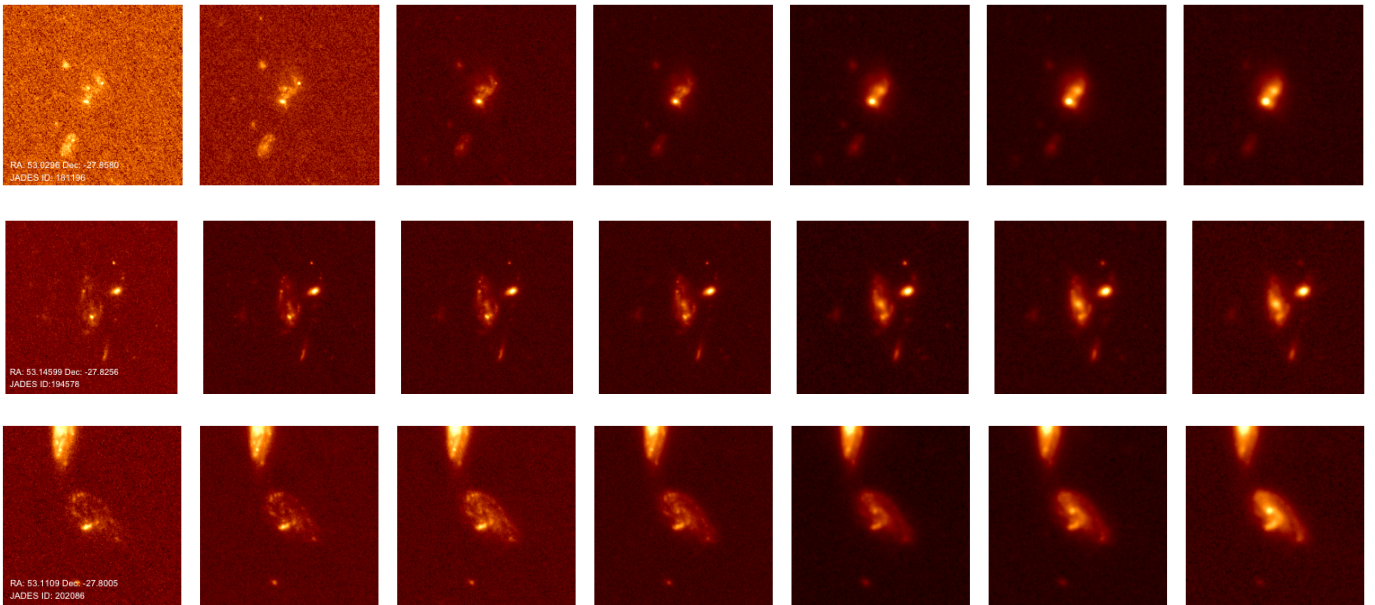


Figure 14. JADES v1 mosaic image cutouts of moderately obscured ($10^{22} < N_H < 10^{23} \text{ cm}^{-2}$) X-ray-selected AGN at $2 < z < 3$ (Lyu et al. 2022) in the following NIRCcam bands: F090W, F115W, F150W, F200W, F277W, F356W, F444W

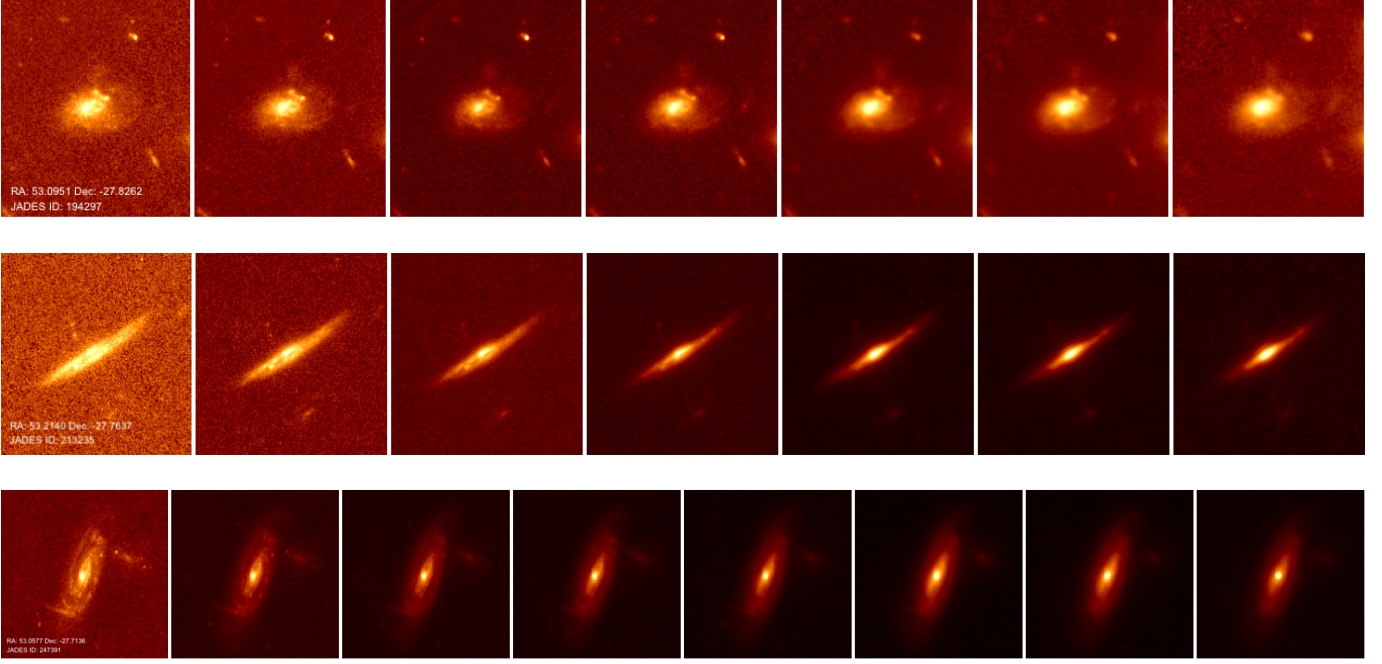


Figure 15. JADES v1 mosaic image cutouts of highly obscured ($N_H > 10^{23} \text{ cm}^{-2}$) X-ray-selected AGN at $0 < z < 1$ (Lyu et al. 2022) in the following NIRCcam bands: (Top, Middle) F090W, F115W, F150W, F200W, F277W, F356W, F444W; (Bottom) F070W, F090W, F115W, F150W, F200W, F277W, F356W, F444W

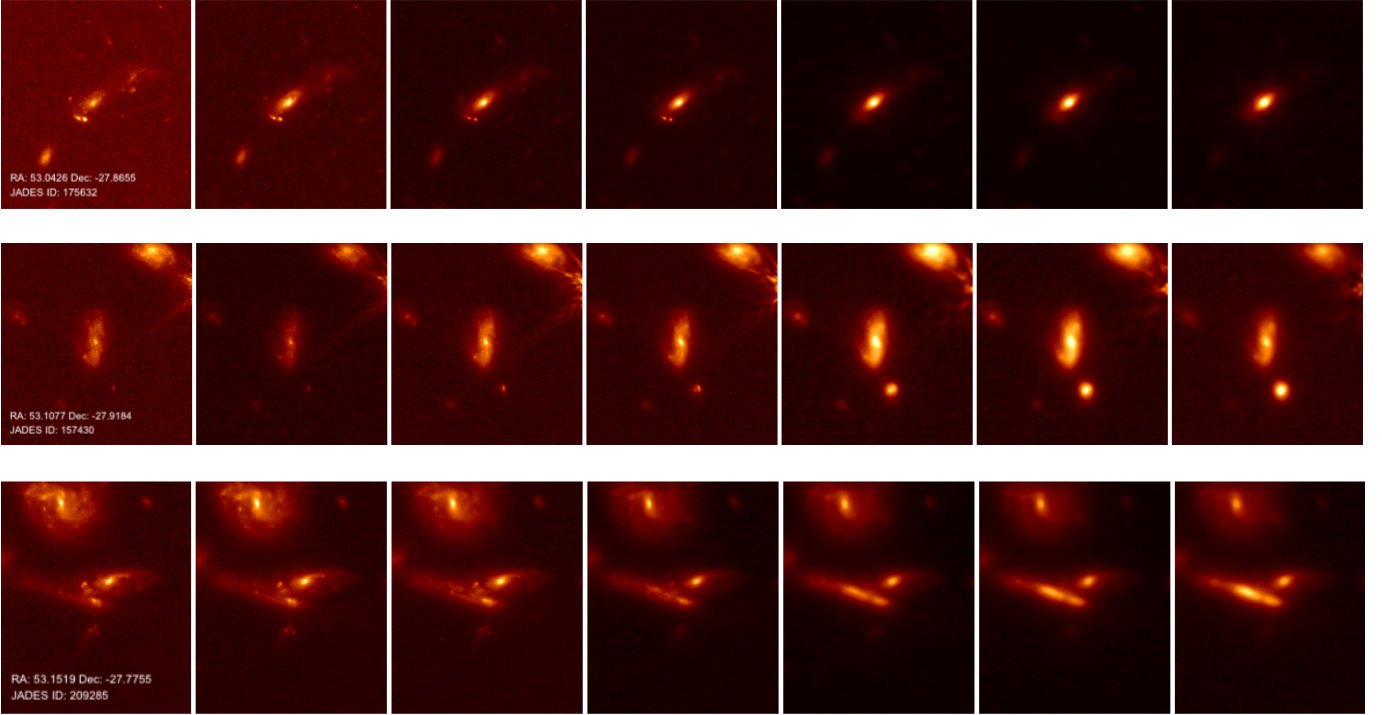


Figure 16. JADES v1 mosaic image cutouts of highly obscured ($N_H > 10^{23} \text{ cm}^{-2}$) X-ray-selected AGN at $1 < z < 2$ (Lyu et al. 2022) in the following NIRCcam bands: F090W, F115W, F150W, F200W, F277W, F356W, F444W

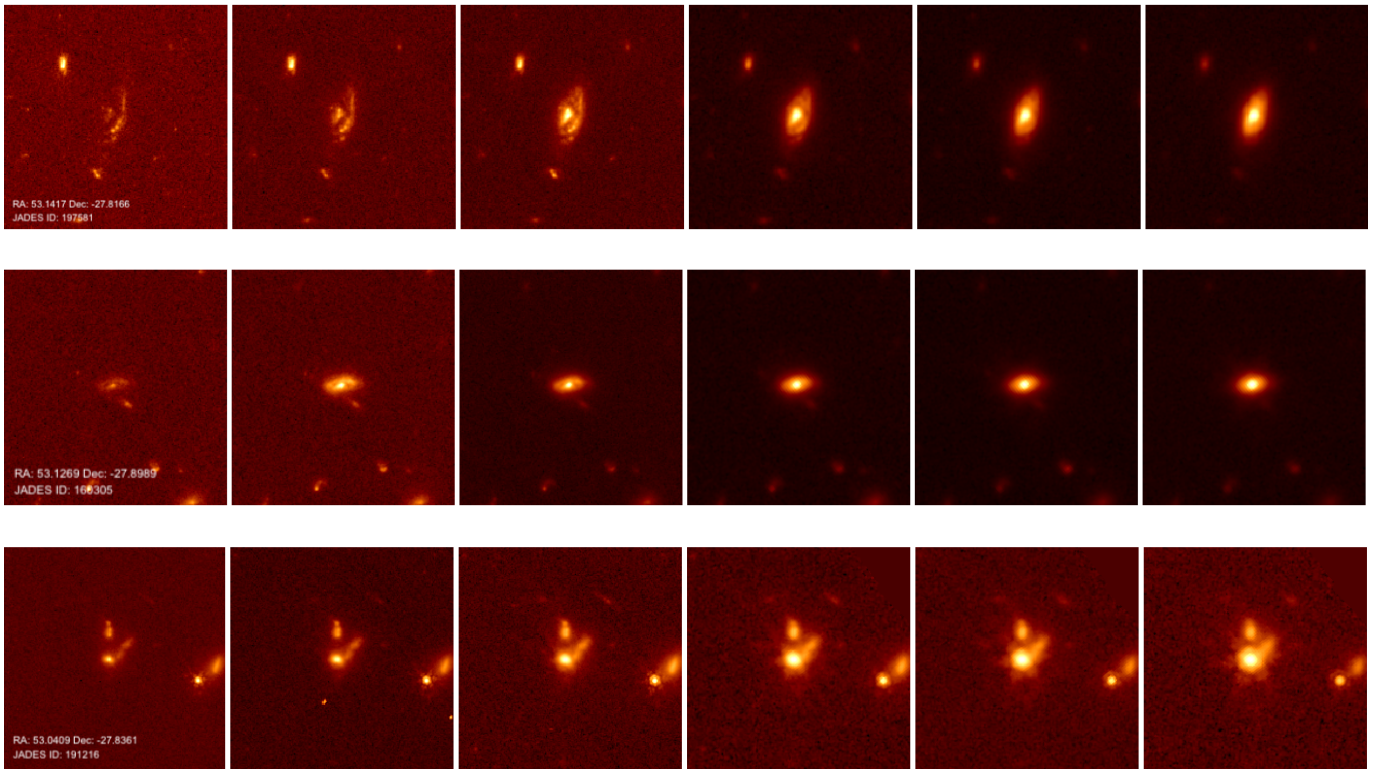


Figure 17. JADES v1 mosaic image cutouts of highly obscured ($N_H > 10^{23} \text{ cm}^{-2}$) X-ray-selected AGN at $2 < z < 3$ (Lyu et al. 2022) in the following NIRCcam bands: F115W, F150W, F200W, F277W, F356W, F444W

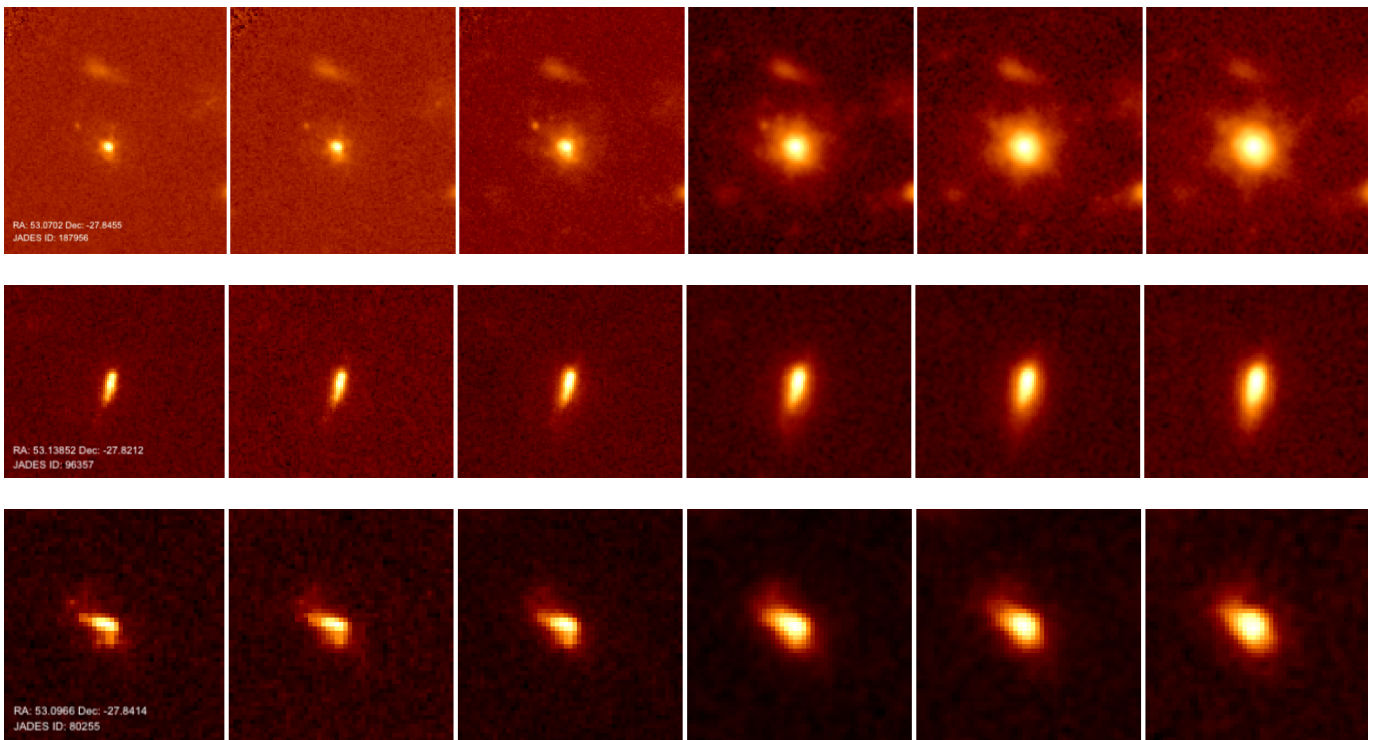


Figure 18. JADES v1 mosaic image cutouts of highly obscured ($N_H > 10^{23} \text{ cm}^{-2}$) X-ray-selected AGN at $3 < z < 4$ (Lyu et al. 2022) in the following NIRCcam bands: F115W, F150W, F200W, F277W, F356W, F444W

1 This work was supported by NASA grants NNX13AD82G, 1255094, and the NASA contract for NIRCcam to the
 2 University of Arizona, NAS5-02015. This work is based on observations made with the NASA/ESA/CSA James
 3 Webb Space Telescope. SA, NB, DJE, KH, ZJ, BR, MR, and CNAW acknowledge support from the NIRCcam Science
 4 Team contract to the University of Arizona, NAS5-02015. DJE is further supported as a Simons Investigator. SA,
 5 JL, IS, and GHR acknowledge support from the JWST Mid-Infrared Instrument (MIRI) Science Team Lead, grant
 6 80NSSC18K0555, from NASA Goddard Space Flight Center to the University of Arizona. These observations are
 7 associated with JWST GTO programs #1180 and #1207, and GO program #1963. AJB acknowledges funding from
 8 the “FirstGalaxies” Advanced Grant from the European Research Council (ERC) under the European Union’s Horizon
 9 2020 research and innovation program (Grant agreement No. 789056). The work of CCW is supported by NOIRLab,
 10 which is managed by the Association of Universities for Research in Astronomy (AURA) under a cooperative agreement
 11 with the National Science Foundation. WB and FDE acknowledge support by the Science and Technology Facilities
 12 Council (STFC) and by the ERC through Advanced Grant 695671 ”QUENCH”.

Facility: JWST

REFERENCES

- Abraham, R. G., Tanvir, N. R., Santiago, B. X., Ellis, R. S., Glazebrook, K., & van den Bergh, S. 1996, *MNRAS*, 279, L47. doi=10.1093/mnras/279.3.L47
- Abraham, R. G., Valdes, F., Yee, H.K.C., & van den Bergh, S. 1994, *ApJ*, 432, 75. doi=10.1086/174550
- Alberts, S., Rujopakarn, W., Rieke, G. H., et al. 2020, *ApJ*, 901, 168. doi=10.3847/1538-4357/abb1a0
- Assef, R. J., Walton, D. J., Brightman, M., et al. 2016, *ApJ*, 819, 111. doi=10.3847/0004-637X/819/2/111
- Bamford, S., et al. 2009, *MNRAS*, 393, 4. doi:10.1111/j.1365-2966.2008.14252.x
- Bershady, M., Jangren, A., & Conselice, C. 2000, *AJ*, 119, 2645. doi=10.1086/301386
- Bignone, L. A., et al. 2017, *MNRAS*, 465, 1. doi=10.1093/mnras/stw2788
- Blecha, L., Snyder, G. F., Satyapal, S., et al. 2018, *MNRAS*, 478, 3056. doi=10.1093/mnras/sty1274
- Bottrell, C., et al. 2023, *MNRAS*, doi=10.1093/mnras/stad2971
- Brinchmann, J., et al. 1998, 499, 1. doi=10.1086/305621
- Bundy, K., Ellis, R., & Conselice, C. 2005, *ApJ*, 625, 2. doi=10.1086/429549
- Darg, S. et al. 2010, *MNRAS*, 401, 2
- Conselice, C., Bershady, M., & Jangren, A. 2000, *ApJ*, 529, 886. doi=10.1086/308300
- Conselice, C. 2003, *ApJS*, 147, 1. doi=10.1086/375001
- Christopher J. Conselice, C.J., Yang, C., & Bluck., A.F.L. 2009, *MNRAS*, 394, 4. doi=10.1111/j.1365-2966.2009.14396.x
- Del Moro, A., Alexander, D. M., Bauer, F. E., et al. 2016, *MNRAS*, 456, 2105. doi=10.1093/mnras/stv2748
- Duras, F., et al. 2020, *A&A*, 636, A73. doi=10.1051/0004-6361/201936817
- Fan, L., et al. 2016, *ApJL*, 822:L32. doi:10.3847/2041-8205/822/2/L32
- Ferrarese, L. & Merritt, D. 2000, *ApJL*, 539, L9. doi:10.1086/312838
- Gebhardt, K., Bender, R., Bower, G., et al. 2000, *ApJL*, 539, L13. doi:10.1086/312840
- Gilli, R., Comastri, A., & Hasinger, G. 2007, *A&A*, 463, 79. doi:10.1051/0004-6361:20066334
- Glikman, E., et al. 2015, *ApJ*, 806, 218. doi=10.1088/0004-637X/806/2/218
- Hao, L., et al. 2005, *AJ*, 129, 1795, doi=10.1086/428486
- Henry, A. L., et al. 2008, *ApJ*, 680, L97. doi=10.1086/589944
- Hernández-Toledo, H. M., Cortes-Suárez, E., Vázquez-Mata, J. A., et al. 2023, *MNRAS*, 523, 4164. doi:10.1093/mnras/stad1425
- Hickox, R. C. & Alexander, D. M. 2018, *ARA&A*, 56, 625. doi:10.1146/annurev-astro-081817-051803
- Hopkins, P. F., Somerville, R. S., Hernquist, L., et al. 2006, *ApJ*, 652, 864. doi:10.1086/508503
- Hopkins, P. F., Hernquist, L., Cox, T. J., et al. 2008, *ApJS*, 175, 356. doi:10.1086/524362
- Hopkins, P. F., Cox, T. J., Younger, J. D., Hernquist, L., et al. 2009, *ApJ*, 691, 2, doi = 10.1088/0004-637X/691/2/1168
- Hopkins, P. F., & Hernquist, L., 2009, *ApJ*, 694, 1, doi=10.1088/0004-637X/694/1/599
- Hopkins, P.F., Kocevski, D. D., Bundy, K., et al. 2014, *MNRAS*, 445, 1. doi:10.1093/mnras/stu1738
- Isserstedt, J., & Schindler, R. 1986, *A&A*, 167, 11.
- Ji, Z., et al. 2022, *ApJ*, 925, 74. doi: 10.3847/1538-4357/ac3837

- Jogee, S. 2006, *Physics of Active Galactic Nuclei at all Scales*, 143. doi:10.1007/3-540-34621-X_6
- Kampczyk, P., et al. 2007, *ApJS*, 172, 329. doi=10.1086/516594
- Kartaltepe, J. S., Mozena, M., Kocevski, D., et al. 2015, *ApJS*, 221, 11. doi:10.1088/0067-0049/221/1/11
- Kim, M., Ho, L. C., Peng, C. Y., et al. 2017, *ApJS*, 232, 21. doi:10.3847/1538-4365/aa8a75
- Kocevski, D. D., Faber, S. M., Mozena, M., et al. 2012, *ApJ*, 744, 148. doi:10.1088/0004-637X/744/2/148
- Kocevski, D. D., Brightman, M., Nandra, K., et al. 2015, *ApJ*, 814, 104. doi:10.1088/0004-637X/814/2/104
- Kormendy, J., & Kennicutt, R. C., Jr. 2004, *ARA&A*, 42, 603. doi:10.1146/annurev.astro.42.053102.134024
- Lintott, Chris J., et al. 2008, *MNRAS*, 389, 3. doi:10.1111/j.1365-2966.2008.13689.x
- Lotz, J. M., Primack, J., Madau, P., 2004, *AJ*, 128, 163, doi=10.1086/421849
- Lotz, J. M., et al. 2010, *MNRAS*, 404. doi=10.1111/j.1365-2966.2010.16268.x
- Lotz, J. M., et al. 2008, *ApJ*, 672, 1. doi=10.1086/523659
- Luo, B., Brandt, W. N., Xue, Y. Q., et al. 2017, *ApJS*, 228, 2. doi:10.3847/1538-4365/228/1/2
- Lyu, J., Alberts, S., Rieke, G. H., et al. 2022, *ApJ*, 941, 191. doi:10.3847/1538-4357/ac9e5d
- Lyu, J., Alberts, S., Rieke, G. H., et al. 2023, arXiv:2310.12330. doi:10.48550/arXiv.2310.12330
- McAlpine, S., et al. 2020, 494, 4. doi=10.1093/mnras/staa1123
- Pawlik, M. M., Wild, V., Walcher, C. J., et al. 2016, *MNRAS*, 456, 3032. doi:10.1093/mnras/stv2878
- Pierce, J. C. S., Tadhunter, C., Ramos Almeida, C., et al. 2023, *MNRAS*, 522, 1736. doi:10.1093/mnras/stad455
- Reza, M., et al. 2021, *Astronomy and Computing*, 37, 100492. doi:10.1016/j.ascom.2021.100492
- Rieke, M. J., Robertson, B. E., Tacchella, S., et al. 2023, arXiv:2306.02466. doi:10.48550/arXiv.2306.02466
- Robertson, B., et al., *ApJ*, 645, 986. doi=10.1086/504412
- Rodriguez-Gomez, V., et al. 2019, *MNRAS*, 483, 4140. doi:10.1093/mnras/sty3345
- Sanders, D. B. & Mirabel, I. F. 1996, *ARA&A*, 34, 749. doi:10.1146/annurev.astro.34.1.749
- Schade, D., Lilly, S. J., Crampton, D., Hammer, F., LeFevre, O., & Tresse, L. 1995, *ApJ*, 451, L1. doi=10.1086/309677
- Shah, E. A., Kartaltepe, J. S., Magagnoli, C. T., et al. 2020, *ApJ*, 904, 107. doi:10.3847/1538-4357/abbf59
- Snyder, G. F., et al. 2015, *MNRAS*, 451, 4290. doi=10.1093/mnras/stv1231
- Suess, K. A., et al. 2022, *ApJL*, 937, L33. doi=10.3847/2041-8213/ac8e06
- Takamiya, M. 1999, *ApJS*, 122, 1. doi=10.1086/313216
- Treister, E., Schawinski, K., Urry, C. M., et al. 2012, *ApJL*, 758, L39. doi:10.1088/2041-8205/758/2/L39
- Tremaine, S., Gebhardt, K., Bender, R., et al. 2002, *ApJ*, 574, 740. doi:10.1086/341002
- Urbano-Mayorgas, J. J., Villar-Martín, M., & Buitrago, F. 2019, *Highlights on Spanish Astrophysics X*, 232
- Villforth, C. 2023, *The Open Journal of Astrophysics*, 6, 34. doi:10.21105/astro.2309.03276
- Walmsley, M., et al. 2022, *MNRAS*, 509, 3. doi:10.1093/mnras/stab2093
- Williams, C.C., et al. 2023, *ApJ*, 268, 64. doi:10.3847/1538-4365/acf130
- Wu, K. 1999, Ph.D. thesis, Univ. California, Santa Cruz
- Xu, L., Rieke, G. H., Egami, E., et al. 2015, *ApJ*, 808, 159. doi:10.1088/0004-637X/808/2/159
- Zakamska, N. L., Strauss, M. A., Heckman, T. M., et al. 2004, *AJ*, 128, 1002. doi:10.1086/423220
- Zakamska, N. L., Sun, A.-L., Strauss, M. A., et al. 2019, *MNRAS*, 489, 497. doi:10.1093/mnras/stz2071
- Zhang, Z., Shi, Y., Rieke, G. H., et al. 2016, *ApJL*, 819, L27. doi:10.3847/2041-8205/819/2/L27